Title: **A conserved chronobiological complex times *C. elegans* development**

Rebecca K. Spangler[1]*, Guinevere E. Ashley[2]*, Kathrin Braun[3]*, Daniel Wruck[1], Andrea Ramos-Coronado[1], James Matthew Ragle[2], Vytautas Iesmantavicius[3], Daniel Hess[3], Carrie L. Partch[1], Helge Großhans[3,4]‡, Jordan D. Ward[2]‡

[1]Department of Chemistry and Biochemistry, University of California-Santa Cruz, Santa Cruz, CA 95064, USA.

[2]Department of Molecular, Cell, and Developmental Biology, University of California-Santa Cruz, Santa Cruz, CA 95064, USA.

[3]Friedrich Miescher Institute for Biomedical Research, 4058 Basel, Switzerland

[4]University of Basel, 4002 Basel, Switzerland

‡Author for correspondence.

*These authors contributed equally to this work

Abstract

The mammalian PAS-domain protein PERIOD (PER) and its *C. elegans* orthologue LIN-42 have been proposed to constitute an evolutionary link between two distinct, circadian and developmental, timing systems. However, while the function of PER in animal circadian rhythms is well understood molecularly and mechanistically, this is not true for the function of LIN-42 in timing rhythmic development. Here, using targeted deletions, we find that the LIN-42 PAS domains are dispensable for the protein's function in timing molts. Instead, we observe arrhythmic molts upon deletion of a distinct sequence element, conserved with PER. We show that this element mediates stable binding to KIN-20, the *C. elegans* CK1δ/ε orthologue. We demonstrate that CK1δ phosphorylates LIN-42 and define two conserved helical motifs, CK1δ-binding domain A (CK1BD-A) and CK1BD-B, that have distinct roles in controlling CK1δ-binding and kinase activity *in vitro*. KIN-20 and the LIN-42 CK1BD are required for proper molting timing *in vivo*. These interactions mirror the central role of a stable circadian PER–CK1 complex in setting a robust ~24-hour period. Hence, our results establish LIN-42/PER – KIN-20/CK1δ/ε as a functionally conserved signaling module of two distinct chronobiological systems.

Introduction

Chronobiology is the study of biological rhythms. Circadian rhythms which enable organisms to anticipate daily cycles of light, temperature, and other environmental variables are one of the best studied examples (Takahashi, 2017). PERIOD (PER) proteins are central to this timekeeping mechanism. Their cellular abundance, stability, and nuclear localization changes rhythmically over a ~24-hour cycle. In mammals, the paralogs PERIOD1 and PERIOD2 (PER1 and PER2) associate with Casein kinase 1 δ/ε (CK1δ/ε) as well as the CRYPTOCHROME proteins, CRY1 and CRY2, to form nuclear transcriptional complexes which repress the transcriptional activators circadian locomotor output cycles protein kaput (CLOCK) and brain and muscle ARNT-like 1 (BMAL1) (Fig. S1A)(Gallego & Virshup, 2007; Gekakis *et al*, 1998; Lee *et al*, 2001; Lowrey & Takahashi, 2011). Since the targets of the CLOCK-BMAL1 heterodimer include PER and CRY themselves, PER and CRY thus eventually repress their own production, permitting subsequent re-expression of CLOCK-BMAL1 to start a new cycle (Gallego & Virshup, 2007; Preußner & Heyd, 2016).

To maintain the 24-hour period of circadian rhythms, a delay between the activation and the repression of CLOCK-BMAL1 transcription is required. Central to this delay is the post-translational modification of PER by one of the two closely related CK1δ and CK1ε kinases. For convenience and because of the redundancy in their function, we will henceforth refer to the two isoforms generically as CK1. Anchored through a CK1-Binding Domain (CK1BD), CK1 is associated with PER for its entire existence in the cell, even translocating from the cytoplasm to the nucleus together (Fig. S1A)(Aryal *et al*, 2017; Lee *et al*, 2001), allowing PER to deliver CK1 to other targets at clock-controlled promoters (Cao *et al*, 2021; Aryal *et al*, 2017). CK1-mediated phosphorylation of a PER degron licenses PER ubiquitylation and subsequent degradation, thereby limiting PER abundance and its period of activity (Fig. S1B)(Akashi *et al*, 2002; Eide *et al*, 2005; Shirogane *et al*, 2005). In addition to the degron, CK1 phosphorylates multiple serines in another PER sequence element known as FASP (“Familial Advanced Sleep Phase”)(Fig. S1B)(Narasimamurthy *et al*, 2018; Philpott *et al*, 2023). Phosphorylation of the FASP site turns PER into an inhibitor of CK1 kinase activity (Philpott *et al*, 2020; Toh *et al*, 2001; Xu

62 *et al*, 2007). In humans, a single residue mutation in this region that blocks all FASP
63 phosphorylation results in a short circadian period then manifests as the eponymous
64 Familial Advanced Sleep Phase, where affected individuals wake up very early in the
65 morning (Jones *et al*, 1999).

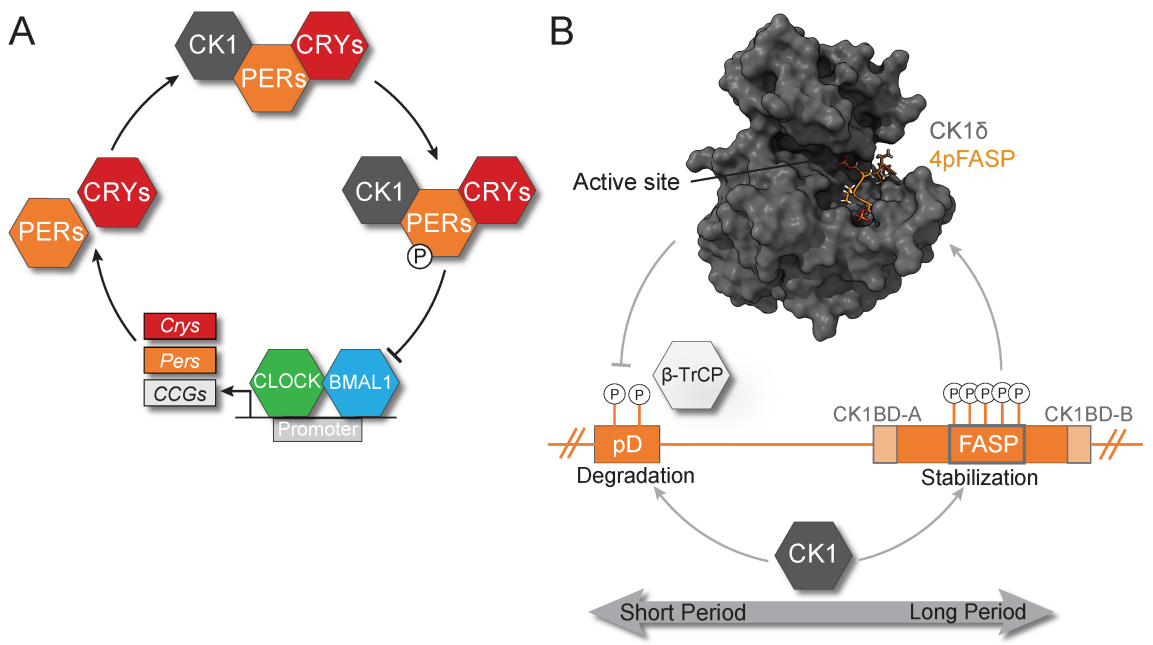

Figure S1. PER proteins have a crucial role in mammalian circadian rhythms. (A) Cartoon schematic of the primary transcription-translation feedback loop which generates ~24-hour rhythms in mammals. CCGs, Clock-controlled genes. **(B)** Cartoon schematic illustrating the mammalian phosphoswitch that dictates CK1-dependent regulation of PER stability. Crystal structure of human CK1δ (gray) bound to phosphorylated PER2 FASP (orange, 4pFASP) peptide, PDB: 8d7o. pD, phosphodegron; FASP, Familial Advanced Sleep Phase.

66 In contrast to circadian timing, the chronobiology of development is mechanistically less
67 well understood. In *C. elegans*, a single PER orthologue, LIN-42, appears to diverge
68 substantially in structure and function from the mammalian and fly PER proteins (Jeon *et*
69 *al*, 1999; Tennessen *et al*, 2006; Monsalve *et al*, 2011). At 598 amino acids for its longest
70 isoform, LIN-42 is substantially shorter than e.g. mouse PER2 at 1225 amino acids (Jeon
71 *et al*, 1999). LIN-42 lacks a CRY-binding domain, consistent with a lack of CRY orthologue
72 in *C. elegans*, and in its tandem PER-ARNT-SIM (PAS) domains, only PAS-B is well
73 conserved, adopts a canonical fold, and mediates dimerization in a mode identical to
74 mammalian PER (Lamberti *et al*, 2023; Migliori *et al*, 2023). Finally, two stretches of
75 sequence, previously termed SYQ and LT according to their first amino acids (Tennessen
76 *et al*, 2006), bear sequence homology to the two PER CK1BD subdomains, CK1BD-A

77 and CK1BD-B, but their function has remained unexplored. *lin-42* further differs from
78 canonical PERs in its expression dynamics and functions: rather than exhibiting a ~24-
79 hour, temperature-invariant period, *lin-42* expression cycles exhibit a temperature-
80 dependent length which can be as short as ~7-hours at 25˚C (Jeon *et al*, 1999;
81 Gissendanner *et al*, 2004). Indeed, *lin-42* was identified as a developmental gene whose
82 mutation causes heterochronic phenotypes, i.e., defects in temporal cell fate specification
83 where cells adopt adult cell fates precociously, in larvae (Abrahante *et al*, 1998; Liu,
84 1990). Hence, it was proposed that *lin-42/PER* constitute an evolutionary link between
85 two distinct, circadian and developmental, timing systems (Jeon *et al*, 1999).

86 The extent of functional similarity between these timing systems generally, and LIN-42
87 and PER function specifically, has remained uncertain, despite the realization that
88 additional orthologues of mammalian clock genes exist and cause heterochronic
89 phenotypes when mutated (Banerjee *et al*, 2005; Gissendanner *et al*, 2004; Jeon *et al*,
90 1999; Kostrouchova *et al*, 1998; Hasegawa *et al*, 2005; Migliori *et al*, 2023). Conceptually,
91 whereas mutations of circadian clock genes such as *PER* change the tempo and/or
92 robustness of circadian rhythms, heterochronic mutations are defined by their ability to
93 alter the sequence of developmental events, such that certain events are skipped
94 (Ambros & Horvitz, 1984; Ambros, 1989). Accordingly, and despite its rhythmic
95 expression, the heterochronic function of LIN-42 does not appear to involve recurring
96 activity but rather the stage-specific repression of the *let-7* miRNA prior to the third larval
97 stage (McCulloch & Rougvie, 2014; Perales *et al*, 2014).

98 LIN-42 is also required for the rhythmic occurrence of molts. Wild-type animals molt, i.e.,
99 regenerate a new collagenous apical extracellular matrix (cuticle), at the end of each of
100 the four larval stages (Lažetić & Fay, 2017). Under constant environmental conditions,
101 individually grown animals enter and exit molts with great temporal uniformity, revealing
102 robust temporal control. *lin-42(ok2385)* mutant animals were shown to cause a slow-down
103 of development as well as an arrhythmic molting phenotype where this uniformity is lost
104 such that individual animals molt at different times (Monsalve *et al*, 2011). It is unknown
105 how LIN-42 contributes to rhythmic molting mechanistically. In addition to *CRY*, the *C.*
106 *elegans* genome lacks obvious orthologues of *BMAL1* and *CLOCK*, arguing for a

107 mechanism that differs from that of the circadian clock at least in the identity of several
108 core components (Hasegawa *et al*, 2005). In a yeast two-hybrid assay, LIN-42 was shown
109 to be capable of binding to numerous transcription factors. Although the functional
110 relevance of such binding for molting has remained unexplored, LIN-42 binding to the
111 REV-ERB orthologue NHR-85 appears important for robust periodic transcription of the
112 heterochronic *lin-4* miRNA (Kinney *et al*, 2023). Finally, loss of KIN-20, the *C. elegans*
113 orthologue of CK1δ/ε, replicates some heterochronic phenotypes of *lin-42* mutation and
114 slows development (Banerjee *et al*, 2005), but its heterochronic functions were argued
115 not to involve LIN-42 (Rhodehouse *et al*, 2018), and it is unknown whether KIN-20 is
116 required for rhythmic molting.

117 Here, we set out to further characterize the molecular and developmental functions of
118 LIN-42. Using targeted mutations, we find that its PAS domains are largely dispensable
119 both for heterochronic pathway activity and rhythmic molting. By contrast, the SYQ/LT
120 regions are specifically required for rhythmic molting. We demonstrate that these domains
121 function as a CK1BD, mediating stable KIN-20/CK1 binding to LIN-42 *in vivo* and *in vitro*.
122 CK1 phosphorylates LIN-42 *in vitro* and this activity is distinctly modulated through the
123 two CK1BD subdomains: CK1BD-B is particularly important for stable CK1 binding,
124 whereas the CK1BD-A element is required for substrate/product inhibition. Our results
125 identify LIN-42/PER–KIN-20/CK1 as a conserved chronobiological complex utilized by
126 two distinct biological oscillators. Although CK1 activity in the circadian clock has
127 previously been viewed mostly through the lens of its effects on PER, our findings align
128 well with the growing notion that PER-mediated regulation of CK1 may be an additional
129 important mechanism to support robust circadian rhythms.

130

131 **Results**

132 **The LIN-42 CK1BD mediates a subset of developmental functions of LIN-42**

133 Previous analysis of the two partial deletion alleles of *lin-42*, *n1089* and *ok2385* (Fig. 1A),
134 have suggested the possibility that different developmental functions could be genetically

135 separable. Although both deletions caused precocious heterochronic phenotypes, only
136 *ok2385* showed evidence of slow and arrhythmic molting (Monsalve *et al*, 2011; Edelman
137 *et al*, 2016; Tennessen *et al*, 2006). To confirm these findings, we quantified molt,
138 intermolt, and larval stage duration for mutant and wild-type animals at high temporal
139 resolution, using an established luciferase assay that monitors entry and exit from the
140 lethargus state associated with molting on animals grown in isolation (Meeuse *et al*, 2020;
141 Olmedo *et al*, 2012). Indeed, we found that *lin-42(ok2385)* mutant larvae developed more
142 slowly than wild-type animals and became increasingly arrhythmic (Fig. 1B). Moreover,
143 most mutant animals underwent only 3 molts (46/48 animals) within the duration of this
144 assay, suggesting either a precocious exit from the molting cycle, or a very delayed or
145 abnormal fourth molt (Fig. 1B). By contrast, essentially all *lin-42(n1089)* animals
146 completed a normal number of molts (54/55 animals) and maintained robust synchrony,
147 although they developed significantly slower than wild-type animals (Fig. 1B). At the same
148 time, both alleles caused robust heterochronic phenotypes, illustrated by precocious
149 formation of alae (Fig. 1C), a cuticular structure normally secreted by terminally
150 differentiated (adult) epidermis in L4 stage larvae.

151 The complex nature of the alleles, each with at least one breakpoint in a noncoding region,
152 precludes a straightforward attribution of the phenotypes to specific features of the LIN-
153 42 protein. Therefore, we decided to generate precise deletions of the two seemingly
154 conserved regions, PAS and SYQ/LT (Fig. 1A). Henceforth, and based on the functional
155 characterization which we describe below, we will refer to SYQ/LT as CK1BD for CK1-
156 Binding Domain. To our surprise, *lin-42(wrd67[ΔPAS])* mutant animals exhibited
157 essentially wild-type molting patterns in the luciferase assay, resembling neither *lin-*
158 *42(n1089)* nor *lin-42(ok2385)* mutant animals. By contrast, *lin-42(wrd63[ΔCK1BD])*
159 mutant animals exhibited increasing loss of molting synchrony over time, akin to *lin-*
160 *42(ok2385)* mutant animals (Fig. 1B). However, *lin-42(ΔCK1BD)* mutant animals
161 executed four detectable molts during the assay (Fig. 1B).

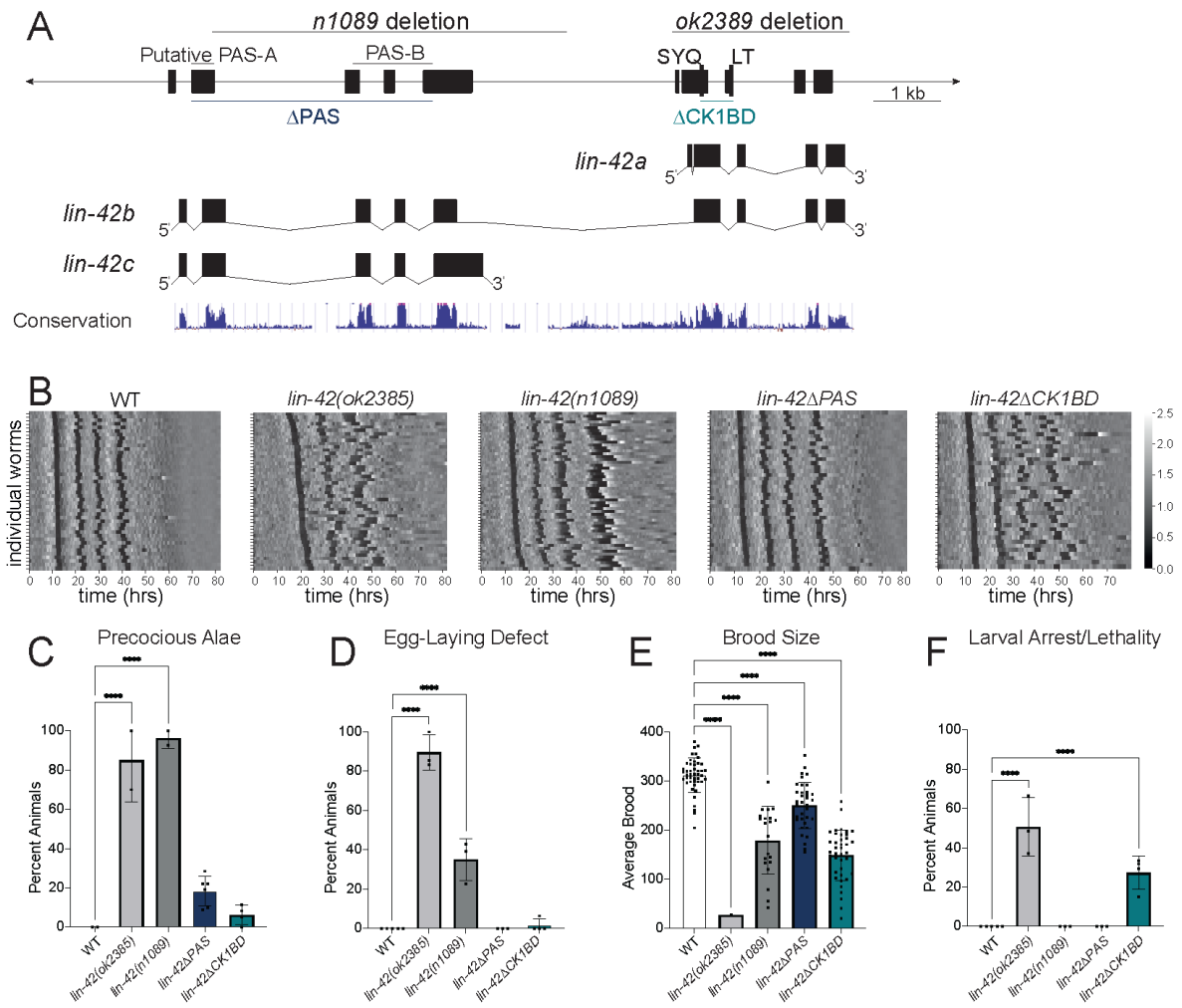

Figure 1. *lin-42* ΔPAS mutants have mild heterochronic phenotypes while ΔCK1BD mutants exhibit asynchronous molting (A) Schematic detailing *lin-42* genomic locus. The gene structure of the *lin-42 a, b*, and *c* isoforms are shown. The location of sequences encoding putative PAS-A, PAS-B, SYQ, and LT domains are indicated. Our ΔPAS and ΔCK1BD CRISPR deletions are indicated in navy and teal, respectively. A track from the UCSC genome browser of conservation with 125 nematode species is below the gene model. **(B)** Heatmaps showing trend-corrected luminescence traces from the indicated genotype. Each line represents one animal. Traces are aligned to the entry of the first molt. Darker color indicates low luminescence signal and corresponds to the molts. **(C)** Bar plot quantifying the percentage of animals of the indicated genotype that prematurely developed a complete or partial alae at the L3-L4 molt. **(D)** Bar plot quantifying the percentage of animals of the indicated genotype that exhibited egg-laying defects as determined by the presence of hatched larvae in the animal. **(E)** Bar plot quantifying the number of larvae of the indicated genotype. **(F)** Bar plot quantifying the percentage of animals of the indicated genotype that arrested or died as larvae. (C-F) Ordinary one-way ANOVA, *p≤0.05 (n≥3, mean ± s.d from two independent strain isolates).

To get a better understanding of the developmental relevance of each domain, we examined additional phenotypes (Fig. 1D-F; Table S1). We found that all four alleles affected brood sizes, albeit to varying degrees, in the order *ok2385>>ΔCK1BD≈n1089>ΔPAS* of decreasing severity (Fig. 1E, Table S1). By contrast,

166 only *ok2385* and *n1089* caused highly penetrant egg-laying (Egl) and precocious alae
167 defects, consistent with previous studies (Fig. 1C and D, Table S1)(Monsalve *et al*, 2011;
168 Edelman *et al*, 2016; Tennessen *et al*, 2006). In contrast, ∆PAS and ∆CK1BD mutants
169 had completely wild-type egg laying and only modest precocious alae. Finally, both
170 *ok2385* and, to a lesser extent, ∆CK1BD caused larval arrest and lethality, a phenotype
171 interestingly not observed in the luciferase assay, suggesting an environmental
172 dependency (Fig. 1F, Table S1). Taken together, these results indicate surprisingly mild
173 phenotypes upon loss of the LIN-42 PAS region and highlight an important function of the
174 CK1BD for rhythmic molting.

175 **LIN-42 and KIN-20 interact *in vivo***

176 Since the genetic results suggested separable functions of LIN-42, we hypothesized that
177 these could depend on specific interaction partners. To start identifying such interaction
178 partners, we performed anti-FLAG immunoprecipitations on endogenously tagged *lin-*
179 *42(xe321[3xFLAG::lin-42b+c])* mixed-stage animal lysates followed by mass-
180 spectrometry. As a control for non-specific binding, we also performed an anti-FLAG
181 immunoprecipitation in an unrelated strain (*sart-3::GFP::3xFLAG)* (Rüegger *et al*, 2015).
182 We observed a single highly enriched interaction partner for LIN-42: KIN-20 – the
183 orthologue of mammalian CK1δ/ε (Fig. 2A).

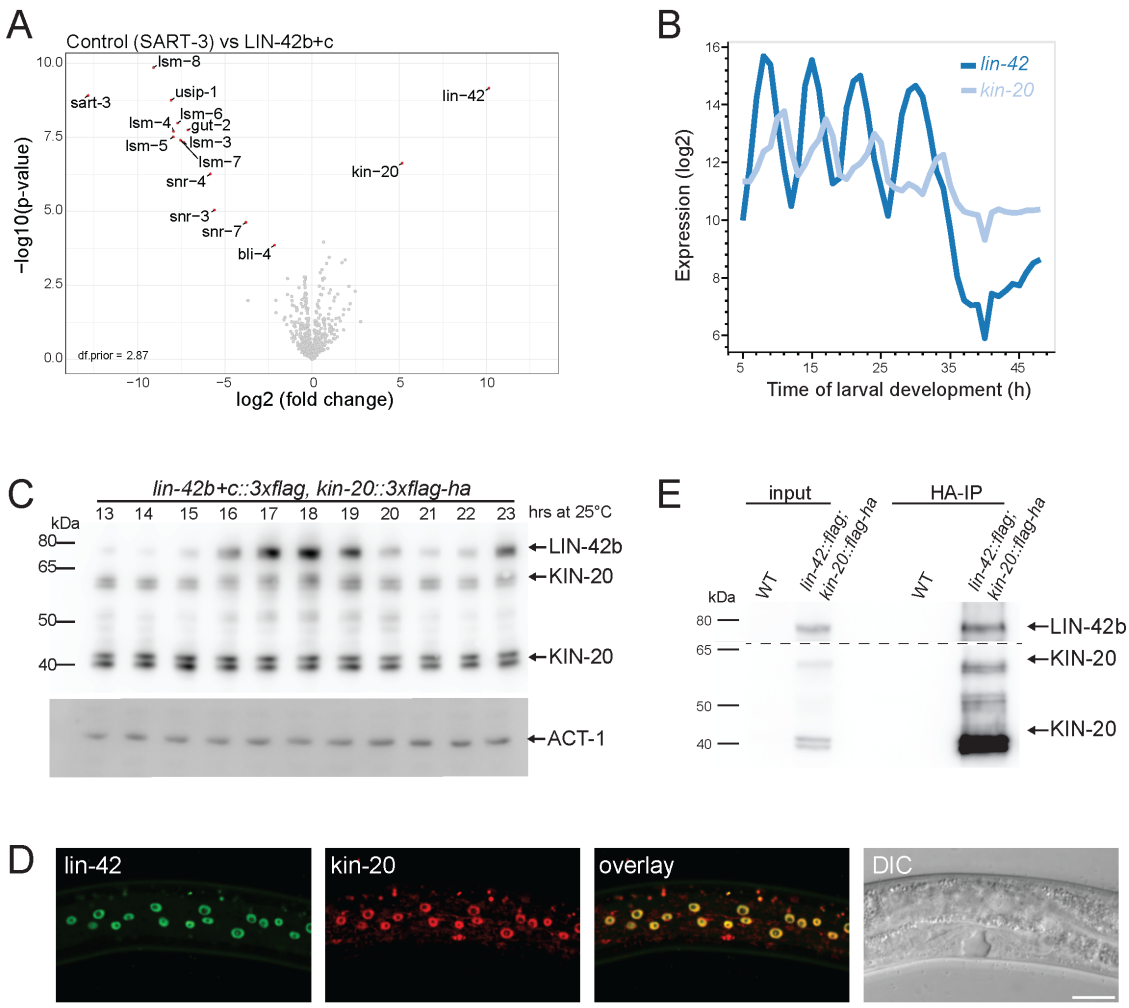

Figure 2. LIN-42 and KIN-20 interact *in vivo* (A) Volcano blot comparing mass spectrometry results from 3xFLAG-LIN-42b+c versus 3xFLAG-SART-3 (control) immunoprecipitations. **(B)** mRNA expression profile for *lin-42* (dark blue) and *kin-20* (light blue) mRNAs throughout larval development. Data Source: Meeuse et al., 2020. **(C)** Western Blot with extracts from *3xflag::lin-42b+c; kin-20::3xflag-ha* (HW3479) larvae collected hourly for 11 hours, starting at 13 h after plating synchronized L1 stage animals on food at 25°C. Top part probed with anti-FLAG-HRP (1:1,000), lower part with anti-actin-1 (1:7,500). Arrows indicate bands for LIN-42b, KIN-20 and ACT-1. **(D)** Confocal images showing the co-localization of GFP::LIN-42b+c and KIN-20::wrmScarlet in the nuclei of epidermal cells. Scale bar = 20μM. **(E)** Anti-HA pulldown from *3xflag::lin-42b+c; kin-20::3xflag-ha* animals. Blot probed with anti-FLAG (1:1,000).

184 The mRNA levels of both *lin-42* and *kin-20* oscillate (Hendriks *et al*, 2014; Meeuse *et al*,
185 2020). Although their peak phases differ, we observed periods where both accumulate.
186 (Fig. 2B). This is also true for the proteins: we observed by Western blotting that the levels
187 of endogenously tagged KIN-20 protein were largely invariant over time, whereas those
188 of endogenously tagged LIN-42b protein levels changed rhythmically (Fig. 2C). Moreover,
189 endogenously tagged KIN-20::wrmScarlet and GFP::LIN-42 proteins co-localized in the

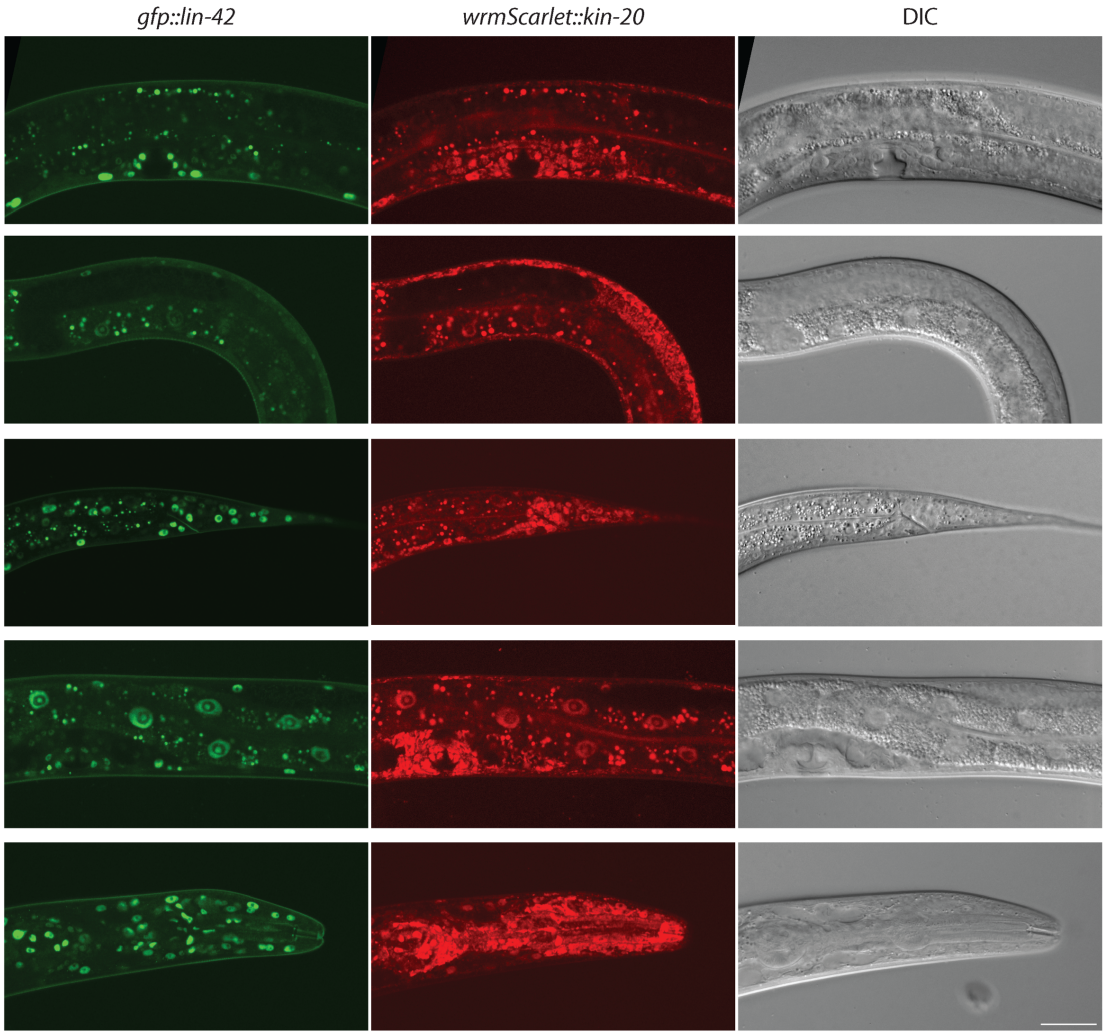

Figure S2. LIN-42::GFP and KIN-20::wrmScarlet expression. Confocal images of endogenously tagged GFP::LIN-42 (green) and KIN-20::wrmScarlet (red) proteins in different tissues. Scale bar = 20μM.

epidermis although, not in some other tissues, where their subcellular localizations differed (Fig. 2D, S2). Finally, we confirmed a physical interaction with a reciprocal anti-HA pulldown from *lin-42(xe321[3xFLAG::lin-42b+c]); kin-20(xe328[3xFLAG-HA::kin-20])* animal lysates, again using endogenously tagged proteins (Fig. 2E). Taken together, we conclude that LIN-42 and KIN-20 mRNA form a complex *in vivo* in at least a subset of tissues.

The LIN-42 SYQ-LT regions form a functional CK1BD capable of binding mammalian CK1

Mammalian CK1 binds PER through its kinase domain, a region that is highly conserved, with CK1δ and KIN-20 exhibiting 79% and 100% sequence identity within the kinase domain and active sites, respectively (Fig. S3)(Dahlberg *et al*, 2009; Crosby *et al*, 2023). By contrast, the CK1BD is less well conserved in LIN-42 with only ~30% sequence identity and a different spacing of the putative LIN-42 CK1BD-A and -B sites (Fig. 3A). Hence, it was unclear whether this region could function as a CK1BD in LIN-42.

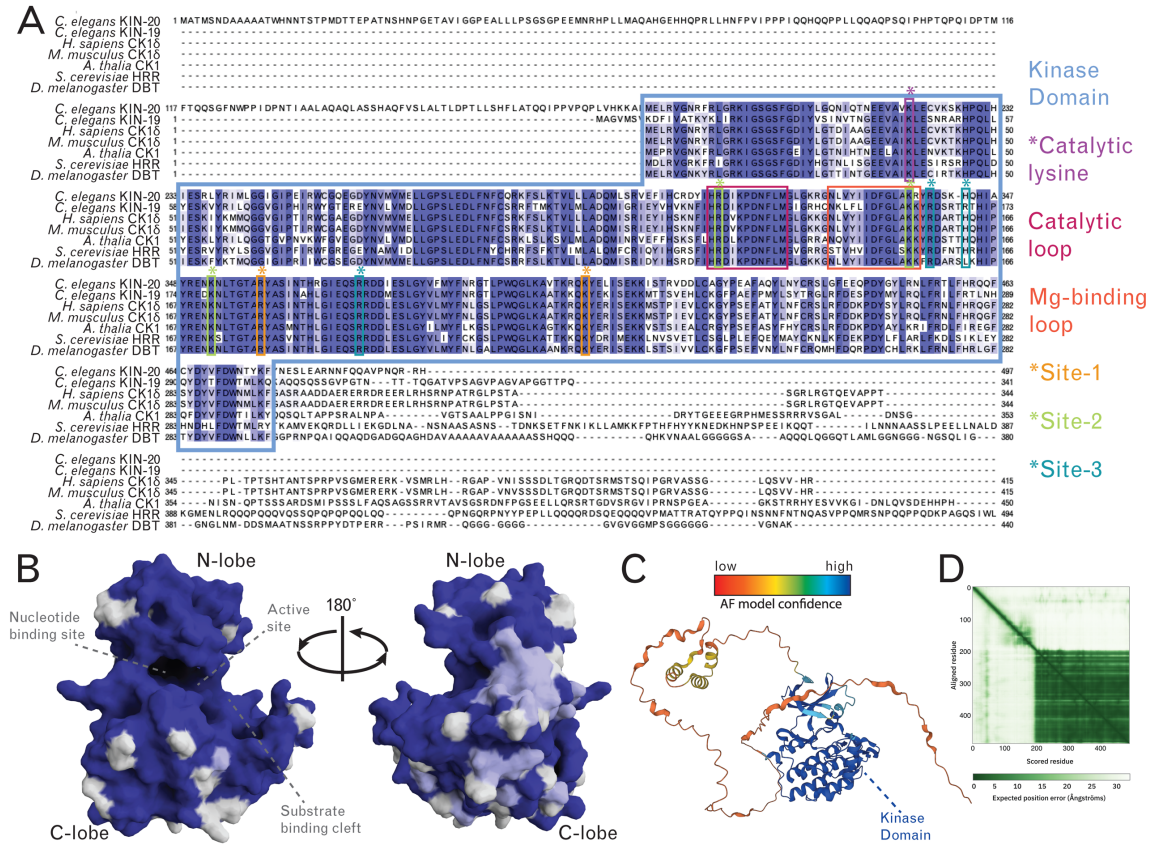

Figure S3. Conservation and structural prediction of *C. elegans* KIN-20 (A) Sequence alignment of *C. elegans* KIN-20 and KIN-19, *H. sapiens* CK1δ, *M. musculus* CK1δ, *A. thalia* CK1, *S. cerevisiae* HRR25 (HRR), and *D. melanogaster* Doubletime (DBT). Important enzymatic sequence features are boxed; full kinase domain (blue box - 79% identical between KIN-20 and human CK1δ), catalytic lysine (purple - conserved in KIN-20), catalytic loop (pink - 100% conserved between KIN-20 and human CK1δ), Magnesium (Mg)-binding loop (orange - 12 out of 13 residues conserved between KIN-20 and human CK1), anion coordination sites 1 (yellow), 2 (green), and 3(blue) (all conserved in KIN-20). **(B)** Crystal structure of *H. sapiens* CK1δ (PDB 6pxo). Dark blue indicates residue is conserved in KIN-20; residues that diverge are highlighted in pale blue (similar amino acid) or not conserved (white). **(C)** AlphaFold structural prediction of KIN-20 (https://alphafold.ebi.ac.uk/entry/A8X4B3) colored by the model confidence. (D) KIN-20 AlphaFold plot of predicted aligned.

We produced recombinant proteins to test this possibility. We were unable to express soluble KIN-20 from a bacterial or insect system, so we used recombinant human CK1δ

206 kinase domain (hereby referred to as CK1), similar to previous studies of KIN-20 (LaBella
207 et al., 2020). *In vitro* pulldown assays with biotinylated LIN-42 protein containing the
208 SYQ/CK1BD-A and LT/CK1BD-B domains as well as C-terminal tail (residues 402-589)
209 revealed that CK1 bound to wild-type LIN-42 protein. Deletion of either the SYQ/CK1BD-
210 1 or LT/CK1BD-B motifs reduced this interaction (Fig. 3B).

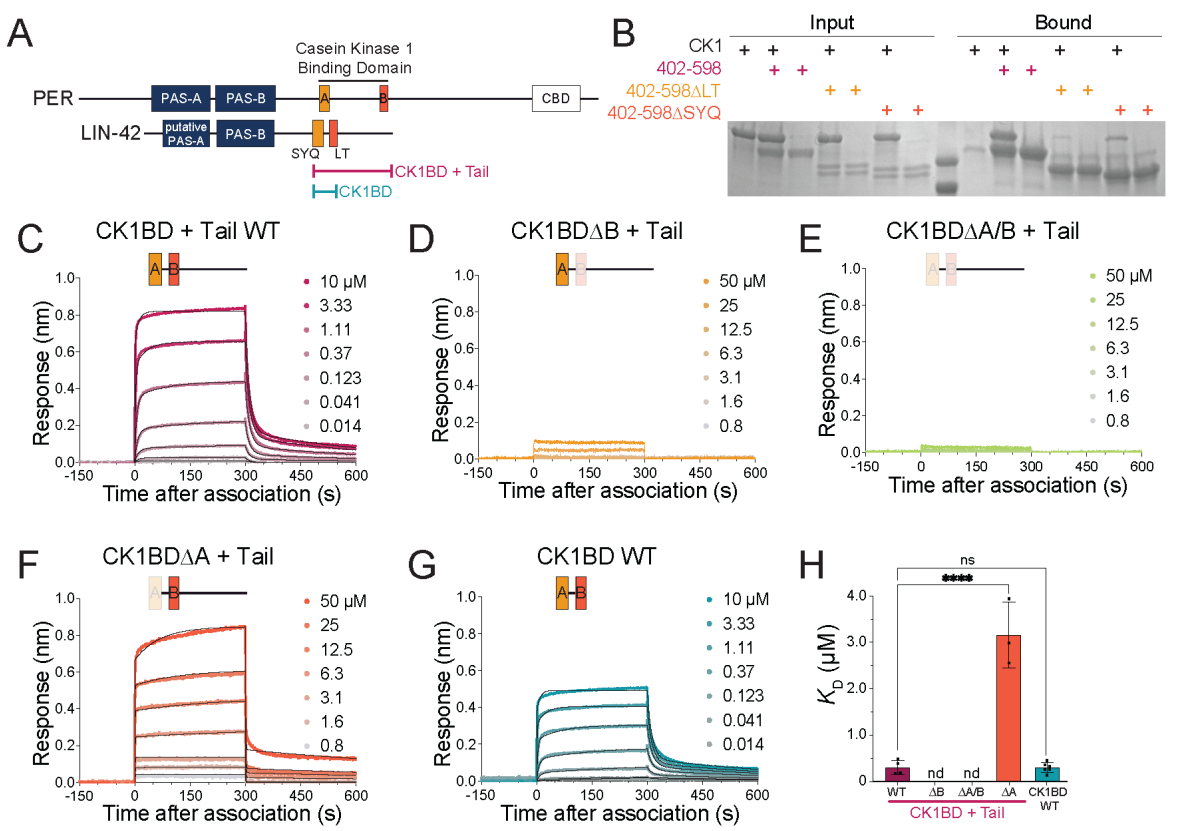

Figure 3. The LIN-42 SYQ and LT domains are a functional CK1-binding domain (A) Schematic representing PER2 and LIN-42 protein domains. Protein constructs used in this study, CK1BD + Tail and CK1BD, are indicated in pink and teal, respectively. CK1BD, Casein Kinase 1-Binding Domain; CBD, CRY-binding domain. **(B)** Representative Co-IP assay of human CK1 and biotinylated LIN-42 CK1BD + Tail proteins. LIN-42 wild-type, SYQ (CK1BD-A) deletion, and LT (CK1BD-B) deletion are indicated in pink, yellow, and orange, respectively. **(C-G)** Bio-layer interferometry (BLI) data for indicated LIN-42 protein binding to immobilized, biotinylated CK1. Inset values represent the concentrations of LIN-42 for individual binding reactions. Model fit to association and dissociation over time represented by black line. Data shown from one representative experiment of n ≥ 3 assays. **(H)** Values for K_D from kinetic analysis of BLI data (C-G) based on a 2:1 heterogeneous ligand binding model and global analysis (Octet). Mean ± SEM, one-way unpaired t-test (p>0.05).

211 To quantitatively analyze this difference in affinity, we performed Bio-Layer Interferometry
212 (BLI) assays, an optical technique that allows for real-time measurement of
213 macromolecular interactions. Using biotinylated CK1 and titrating in various LIN-42
214 fragments to assess differences in CK1 binding, we measured k_{on} and k_{off} rates and

215 subsequently calculated the affinity constant (K_D) for CK1 to the various LIN-42 constructs.
216 The LIN-42 C-terminal fragment (CK1BD+Tail) bound CK1 with nanomolar affinity (K_D=
217 209 ± 78 nM)(Fig. 3C). Despite titrating higher concentrations, LIN-42 binding to CK1 was
218 not detectable when CK1BD-B was deleted, either singly (*CK1BD-ΔB*) or in combination
219 with CK1BD-A (*CK1BD-ΔA/B*) (Fig. 3D,E,H). Deletion of the CK1BD-A domain reduced
220 the affinity of LIN-42 to CK1 approximately 10-fold (K_D = ~3 μM)(Fig. 3F,H), consistent
221 with a need to titrate in higher concentrations of LIN-42 CK1BD-ΔA + Tail protein to
222 calculate an accurate K_D. These data indicate that CK1BD-A and B both contribute to
223 high-affinity binding of CK1 *in vitro*, while revealing the more important contribution of the
224 CK1BD-B motif. This data is consistent with recent work that demonstrated an essential
225 role of the human PER2 CK1BD-B motif for stable association with CK1 in a mouse model
226 and mammalian cells (An *et al*, 2022).

227 To test whether the CK1BD was sufficient to bind CK1, we purified a truncated fragment
228 of LIN-42 lacking the C-terminal tail (CK1BD). Because of its smaller size, this
229 recombinant CK1BD fragment produced a lower response signal compared to CK1BD +
230 Tail protein yet bound CK1 with a comparable, nanomolar affinity (K_D = 348 ± 123 nM)
231 demonstrating that the SYQ and LT domains encompass a minimal CK1BD (Fig 3G,H).
232 We conclude that the LIN-42 CK1BD is functionally conserved and mediates stable
233 binding to the human CK1 kinase domain.

234 **Phosphorylation of the LIN-42 C-terminus by CK1 exhibits a conserved mode of**
235 **feedback inhibition**

236 Mammalian CK1 regulates PER abundance by controlling its degradation post-
237 translationally. Mutations on CK1 or its PER phosphorylation sites can induce changes in
238 circadian period as great as ~4-hours (Akashi *et al*, 2002; Shirogane *et al*, 2005; Eide *et*
239 *al*, 2005; Lowrey *et al*, 2000; Xu *et al*, 2005; Toh *et al*, 2001; Xu *et al*, 2007). To test
240 whether LIN-42 is a CK1 substrate, we performed *in vitro* ^{32}P-ATP kinase assays using
241 the CK1BD alone or the CK1BD + Tail as substrates. CK1BD protein contains 4 serines
242 and 6 threonines while the CK1BD + Tail construct contains an additional 22 serines and
243 15 threonines. We observed phosphorylation for both constructs, yet more robustly on

244 LIN-42 CK1BD + Tail than on CK1BD alone (Fig. 4A-C). Hence, KIN-20 appears capable
245 of phosphorylating both CK1BD and the extended C-terminal tail. Deletion of CK1BD-B
246 reduced phosphorylation relative to the wild-type protein, whereas phosphorylation of the
247 CK1BD-ΔA + Tail mutant protein remained largely unaltered (Fig. 4A-C). Thus, in the two
248 assays, loss of CK1BD-B impacts both binding and phosphorylation by CK1 more strongly
249 than loss of CK1BD-A (Fig. 3D, 4A-C).

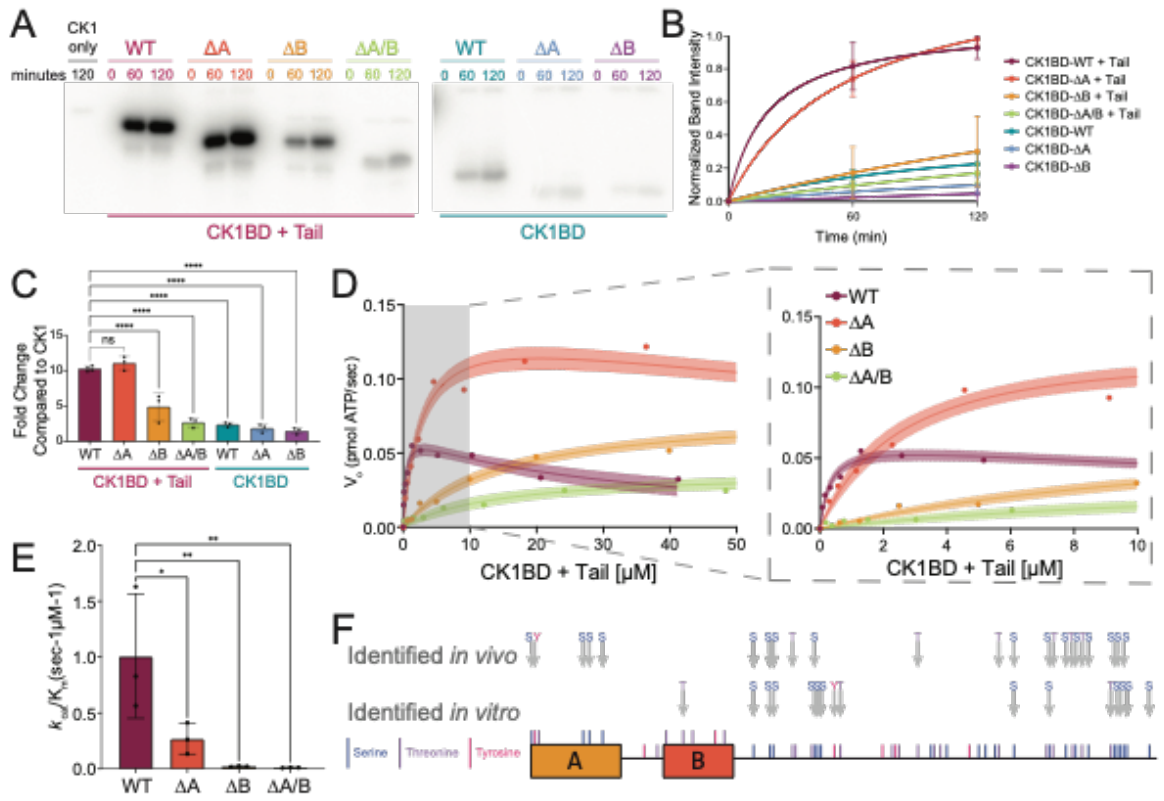

Figure 4. The extended C-terminus of LIN-42 is phosphorylated by CK1 (A) Representative ^{32}P-radiolabeled ATP enzymatic assay of CK1 activity on LIN-42 CK1BD + Tail and CK1BD wild-type and indicated domain deletion mutants. **(B)** Quantification of band intensity depicted in (A) and replicates. Model fit to Michaelis Menten, n = 3. **(C)** Fold change quantification of band intensity from panels A & B compared to CK1 autophosphorylation at 120 minutes. Ordinary one-way ANOVA, *p < 0.05, n ≥ 3, mean ± SEM. **(D)** Representative ADP-Glo enzymatic assay comparing activity of CK1 on LIN-42 CK1BD + Tail wild-type (maroon), CK1BD-ΔA (orange), CK1BD-ΔB (yellow), and CK1BD-ΔA/B (green). **(E)** Values of k_{cat}/K_m calculated from (D). n=3, mean ± SEM, Ordinary one-way ANOVA (p>0.05). **(F)** LIN-42 phosphorylation sites identified via mass spectrometry from *in vivo* samples from whole worm lysate collected hourly from synchronized L1 animals from 14 hrs (early L2) to 25 hrs (late L3) after plating at 25°C (top arrows) *in vitro* kinase reactions of CK1 activity on LIN-42 CK1BD + Tail (bottom arrows). Serine, threonine, and tyrosine residues are indicated via vertical blue, purple, and pink ticks, respectively, along the CK1BD + Tail construct schematic.

250 To explore the kinetics of CK1 phosphorylation of the LIN-42 extended C-terminus, we
251 performed substrate titration experiments using an ADP-Glo enzymatic assay. Here, we

252 observed a decrease in kinase activity with high levels of wild-type LIN-42 CK1BD + Tail
253 (Fig. 4D). This result mirrors the ability of phosphorylated PER as well as the apoptosis
254 substrate p63, to inhibit the activity of CK1 (DBT in Drosophila) in both mammalian and
255 *Drosophila* systems through product inhibition (Philpott et al., 2023).

256 Closer examination revealed that deletion of the LIN-42 CK1BD-A motif relieved feedback
257 inhibition (Fig. 4D), explaining why the ^{32}P-ATP data had shown little decrease in the
258 overall phosphorylation level (Fig. 4A-C) despite having reduced affinity for the kinase
259 (Fig. 3E,F,H). Conversely, deletion of the B motif either in isolation or with the A motif,
260 caused a significant reduction in overall phosphorylation of CK1BD + Tail. No serines and
261 only 4 threonines are removed in this deletion, so this effect was likely not due to loss of
262 phosphosites. The catalytic efficiency (k_{cat}/K_m) of CK1 for each LIN-42 substrate decreased
263 significantly with deletion of the CK1BD motifs relative to wild-type, with activity most
264 severely impacted upon loss of the CK1BD-B motif (Fig. 4D,E). Taken together, these
265 results suggest that while both motifs are involved in binding to CK1, deletion of the
266 CK1BD-A region predominantly relieves feedback inhibition without fully disrupting the
267 anchoring interaction seen with the deletion of the CK1BD-B domain. Moreover, and
268 similar to the mammalian PER–CK1 complex (Marzoll *et al*, 2022), loss of the anchoring
269 interaction compromises, but does not fully abrogate phosphorylation.

270 **Identification of potential LIN-42 phosphosites**

271 To determine potential CK1-dependent LIN-42 phosphorylation sites, we performed *in*
272 *vitro* kinase reactions followed by phosphoenrichment and mass spectrometry to identify
273 phosphopeptides. There are a total of 26 serines and 21 threonines in the CK1BD + Tail
274 construct. We identified 12 serines and 3 threonines in the C-terminus that were
275 phosphorylated upon incubation of LIN-42 CK1BD + Tail with CK1 at least once from
276 three replicates *in vitro* (Fig. 3F). Although we detected low levels of phosphorylation on
277 LIN-42 constructs lacking the tail in the ^{32}P-ATP assay (Fig. 3A), no serine and only one
278 threonine phosphorylation within the CK1BD was detected *in vitro,* reflecting possible
279 limitations in the assays.
280
281

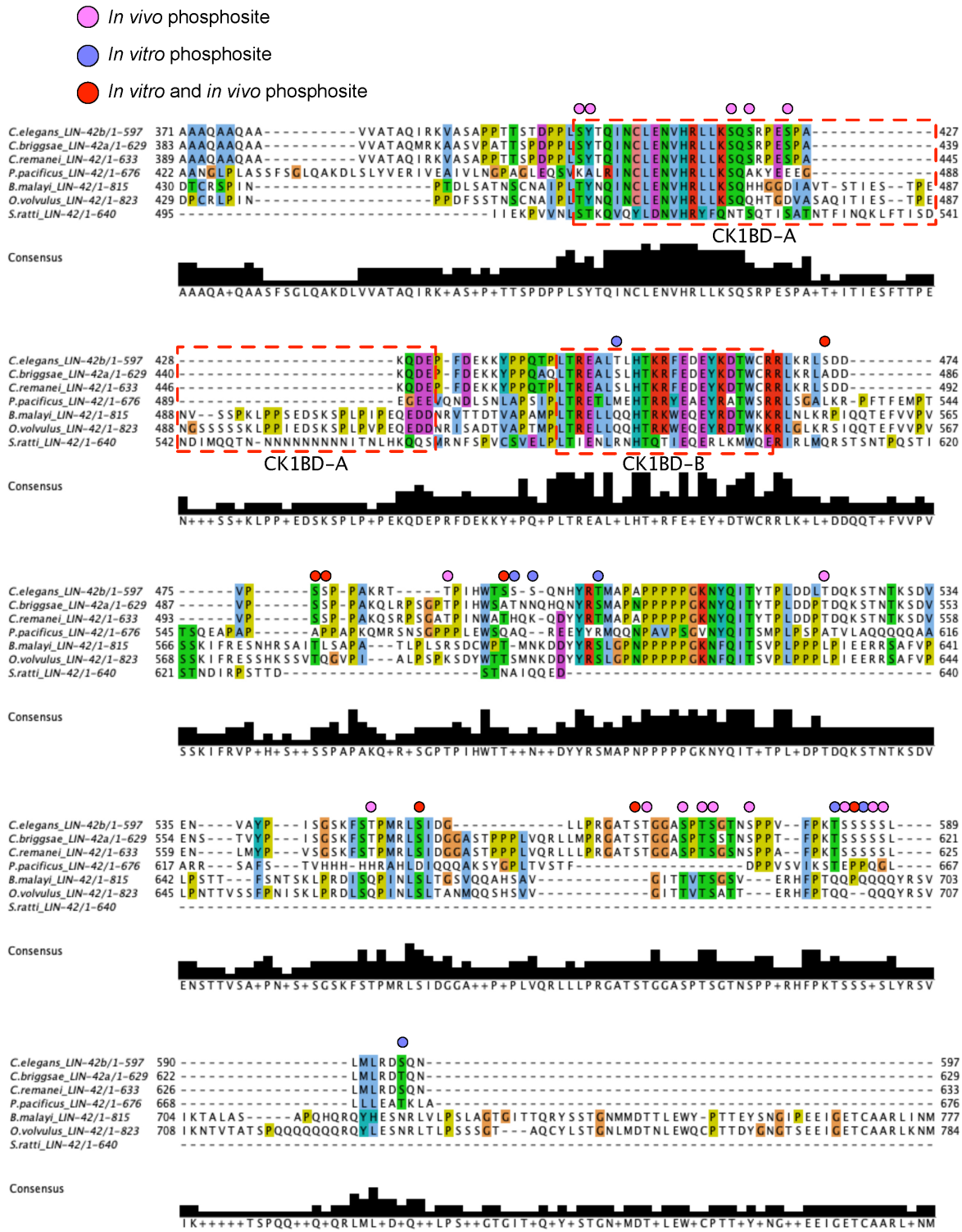

Figure S4. Alignment of the CK1BD and C-terminal tail region of LIN-42 homologs. LIN-42 homologs from the indicated nematode species were aligned using Clustal Omega. The length in amino acids of each homolog follows the species and homolog name. To the left and right of the alignment are amino acid positions of the end residues for each protein. Blue shading indicates conserved sequences and the histogram at the bottom depicts the degree of conservation with a consensus sequence listed below. The positions of the *C. elegans* CK1BD-A and CK1BD-B motifs are indicated. The location of the phosphosites found in our *in vivo*, *in vitro* and both datasets are indicated.

283 To see if LIN-42 was phosphorylated *in vivo*, we immuno-precipitated endogenously
284 tagged 3xFLAG-LIN-42b+c at various time points from a population of synchronized L2
285 stage larvae and subjected precipitates to mass spectrometry. This yielded 16
286 phosphorylated serines and 6 phosphorylated threonines, among which 8 serines
287 overlapped with the 11 phosphoserines identified after *in vitro* reaction while no
288 threonines were observed to be phosphorylated in both the *in vitro* and *in vivo* datasets
289 (Fig. 3F, S4). This overlap of *in vitro* and *in vivo* results is consistent with the possibility
290 that LIN-42 is a CK1 substrate *in vivo*. Whether incomplete overlap reflects differences in
291 kinase activities in the activity of additional kinases and/or specificity factors *in vivo*, or
292 technical differences in the experimental approaches remains to be determined.
293
294 ***kin-20* null and catalytically dead mutants exhibit arrhythmic molting**
295 CK1 binds to and phosphorylates LIN-42 (Fig. 2-4) and loss of the LIN-42 CK1BD causes
296 arrhythmic molting (Fig. 1). Hence, we hypothesized that *kin-20* mutants would partially
297 phenocopy *lin-42(ΔCK1BD)* mutants. Indeed, when we monitored molt timing with the
298 luciferase assay, we found that *kin-20* loss recapitulated both the slow development and
299 arrhythmic molt phenotypes of *lin-42(ok2835)* and *lin-42(ΔCK1DB)* mutations (Fig. 1B;
300 Fig. 5A). The same phenotype was observed with a *kin-20* point mutation engineered to
301 abrogate enzymatic activity of the kinase, D310A, indicating that KIN-20 activity is
302 required for molt timing (Fig. 5A).
303
304 Like *lin-42(ok2835)* and *lin-42(ΔCK1DB)* mutations, a *kin-20(ok505)* loss-of-function
305 mutation also caused larval arrest when animals were grown on plate but not in the liquid
306 culture luciferase assay (Fig. 1F; Fig. 5B). Additionally, we found that *kin-20(ok505)* null
307 mutant animals resembled *lin-42(ok2835)* mutants in their severe egg-laying defects and
308 brood size reduction, phenotypes which are weaker or even absent from *lin-42(ΔCK1DB)*
309 animals (Fig. 1D,E; Fig. 5C,D). Finally, like *lin-42(ΔCK1DB)* animals but unlike *lin-*
310 *42(ok2385)* mutants, *kin-20* null mutants did not develop precocious alae (Fig. 1G; Fig.
311 5E), consistent with earlier work (Banerjee 2005). We conclude that loss of KIN-20 and
312 its CK1BD binding site on LIN-42 cause largely overlapping phenotypes. The more severe
313 phenotypes of *kin-20(ok505)* mutants relative to *lin-42(ΔCK1DB)* animals implicate

314 additional roles for KIN-20 in development and/or may reflect its residual activity on LIN-
315 42ΔCK1BD.
316

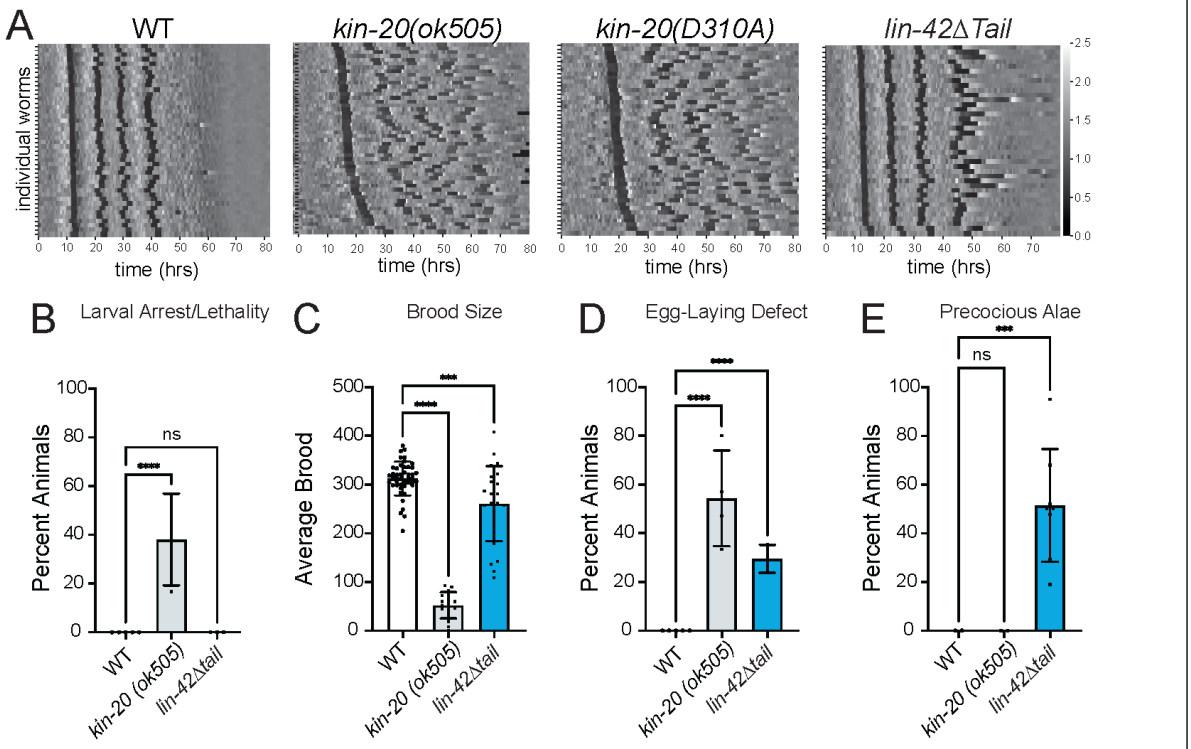

Figure 5. *kin-20* null and catalytically dead alleles exhibit larval arrest and asynchronous molting similar to *lin-42(*ΔCK1BD*)* mutants (A) Heatmaps showing trend-corrected luminescence traces from the indicated genotype. Each line represents one animal. Traces are aligned to the entry of the first molt. Darker color indicates low luminescence signal and corresponds to the molts. **(B)** Bar plot quantifying the percentage of animals of the indicated genotype that arrested or died as larvae. **(C)** Bar plot depicting the average number of live progeny from hermaphrodites of the indicated genotype. **(D)** Bar plot quantifying the percentage of animals of the indicated genotype that exhibited egg-laying defects as determined by the presence of hatched larvae in the animal. **(E)** Bar plot quantifying the percentage of animals of the indicated genotype that prematurely developed a complete or partial alae at the L3-L4 molt. (B-E) all analysis, ordinary one-way ANOVA, *p≤0.05 (n≥3, mean ± s.d from two independent strain isolates).

317 **LIN-42 C-terminal tail deletion causes a heterochronic phenotype but leaves**
318 **molting timing largely unaffected**

319 Finally, to explore the functional relevance of LIN-42 tail phosphorylation *in vivo*, we
320 generated *lin-42(ΔTail)* mutant animals. We found that these animals, which retained the
321 CK1BD, did not recapitulate the *lin-42(ΔCK1DB)* or *kin-20* null mutant phenotypes but
322 instead appeared phenotypically most similar to *lin-42(n1089)* (Fig. 1C-F; Fig. 5).
323 Specifically, *lin-42(ΔTail)* mutants have regular timing of the first three molts, yet an

extended and irregular fourth molt (Fig. 5A). They also exhibited a modest reduction in brood size, egg-laying defects and precocious alae but no larval arrest (Fig. 5B-E). These data indicate that the LIN-42 C-terminus is largely dispensable for timing of larval molting and suggest instead that it plays a role in the heterochronic functions of LIN-42.

Discussion

PER and its nematode orthologue LIN-42 control two distinct types of biological timing: mammalian and fly circadian rhythms (PER) and *C. elegans* developmental timing (LIN-42). The identification of additional orthologous pairs functioning in these respective pathways, ROR/NHR-23, CK1/DBT/KIN-20, Timeless/TIM-1, and REV-ERB/NHR-85, suggests that there is a conserved set of biological timing genes, whose function can be exploited in different contexts. The wiring among these components, in the few cases where this has been explored, appeared strikingly different, making it unclear why and how these genes would be evolutionarily selected for distinct timing functions. Our work shows the first example of a conserved module in these clocks: the LIN-42/PER – KIN-20/CK1 interaction.

The PAS domains are largely dispensable for LIN-42 developmental timing function

The PAS domains are the most notable feature of LIN-42 sequence conservation and were thought to be an interaction platform for a developmental stage-specific binding partner (Jeon *et al*, 1999). Previous work characterizing the *lin-42(ok2385)* and *n1089* alleles suggested that the PAS domains were necessary for the heterochronic functions of LIN-42 (Tennessen *et al*, 2006; Monsalve *et al*, 2011). Yet, our precise deletion of the LIN-42 PAS domains caused only a mild precocious alae phenotype with significantly less penetrance than in *lin-42(n1089)* mutants, suggesting that this model is incorrect. While *lin-42(n1089)* removes the sequence of the PAS domains, it also results in a truncation of *lin-42b* and removal of part of the *lin-42a* promoter sequence (Tennessen *et al*, 2006; Monsalve *et al*, 2011). The *n1089* phenotype could reflect loss of the PAS domains combined with potential reduction in expression of other elements such as the C-terminal tail or an NHR-85 interaction site (Kinney *et al*, 2023).

354 The weak phenotypes seen with our precise deletion are particularly striking when
355 considering that the PAS domains, and specifically the highly conserved PAS-B domain,
356 mediate LIN-42 dimerization (Lamberti *et al*, 2023) - a function that is important for PER
357 activity in circadian rhythms (Zheng *et al*, 1999). Although it remains to be determined
358 whether the PAS domains are necessary for LIN-42 dimerization *in vivo*, it seems possible
359 that LIN-42's molting timing function does not require dimerization.
360
361 **LIN-42 contains a CK1BD that is important for rhythmic molting**
362 Contrasting with the PAS domain, we found the LIN-42 SYQ/LT regions to be required
363 for rhythmic molting, and we could demonstrate *in vitro* that they constitute a functional
364 CK1BD that anchors KIN-20/CK1, promotes LIN-42 phosphorylation, and mediates
365 kinase inhibition. Moreover, the patterns of phosphorylation that CK1 generates on LIN-
366 42 *in vitro* overlap with those that we observed on LIN-42 *in vivo*. We do note that it
367 remains to be demonstrated to which extent the *in vivo* phosphorylations depend on KIN-
368 20. Our attempts to address this question by examining LIN-42 phosphorylation in strains
369 lacking active KIN-20 were thwarted by the slow growth, sickness, and arrhythmic molting
370 observed in these strains.
371
372 The two CK1BD subdomains have separable functions *in vitro*. The CK1BD-B plays a
373 more prominent role in kinase binding, mirroring the anchoring function of its mammalian
374 and *Drosophila* equivalents (Marzoll *et al*, 2022; Philpott *et al*, 2023). Anchoring allows
375 CK1 to target lower affinity, non-consensus motifs, which are key regulatory sites in
376 fly/mammalian clocks (Marzoll *et al*, 2022; Philpott *et al*, 2023; An *et al*, 2022; Nawathean
377 *et al*, 2007; Kim *et al*, 2007). However, without the PER CK1BD-B not all capacity for
378 phosphorylation is lost, which suggests that high-affinity binding is not essential for
379 phosphorylation but promotes it (Marzoll *et al*, 2022). For LIN-42-ΔCK1BD-B, we also see
380 low levels of phosphorylation by CK1 *in vitro* (Fig. 4), suggesting that it may play a similar
381 role in controlling KIN-20 activity.
382
383 The LIN-42 CK1BD-A plays a less prominent role in binding but rather is involved in CK1
384 inhibition. CK1δ-dependent phosphorylation of both mammalian and *Drosophila* PER at

385 sites near the CK1BD leads to feedback inhibition of CK1 through conserved anion
386 binding sites (Philpott *et al*, 2023). Our *in vitro* LIN-42 phosphorylation data reveal a
387 decrease in enzyme catalytic activity as substrate concentration increases, dependent on
388 the CK1BD-A, consistent with feedback product inhibition of KIN-20 (Fig. 4). Alternatively,
389 this result could reflect substrate inhibition, where increasing amounts of LIN-42
390 CK1BD+Tail result in a non-productive enzyme-substrate complex. Such substrate
391 inhibition has also been reported in several recent studies of CK1 showing
392 phosphorylated substrates binding the enzyme and regulating its activity (Gebel *et al*,
393 2020; Cullati *et al*, 2022; Harold *et al*, 2023; Crosby *et al*, 2023). Further enzymatic and
394 structural studies will be required to distinguish between these modes of regulation.
395
396 **Function of the LIN-42-CK1 interaction**
397 Many models of circadian clock function highlight phosphorylation of PER by CK1 as the
398 central consequence of their interaction, controlling PER stability and thereby setting the
399 period length. Intriguingly, although CK1 heavily phosphorylates the LIN-42 C-terminal
400 tail, including on serines and threonines that are conserved among *Caenorhabditis*
401 nematodes, but not on more distantly related nematodes (Fig. S4), deletion of this
402 sequence does not affect molting rhythmicity. These data suggest either phosphosite
403 redundancy, or that regulated phosphorylation of LIN-42 is not the key function of this
404 complex for controlling molting timing.
405
406 For PER–CK1, several lines of evidence show that reciprocal to CK1-mediated regulation
407 of PER, PER also regulates CK1 activity, both on itself and potentially other targets such
408 as CLOCK. Indeed, PER and CRY function as a bridging complex to provide CK1 access
409 to CLOCK (Cao *et al*, 2021; Aryal *et al*, 2017), and although the CK1BD is not absolutely
410 required for PER phosphorylation (Kim *et al*, 2007), its mutation causes defects in PER
411 nuclear localization and CK1-mediated phosphorylation of CLOCK (Cao *et al*, 2021;
412 Chiou *et al*, 2016). Product inhibition through phosphorylated PER may thus limit
413 phosphorylation not only of PER itself, but potentially also of other substrates, including
414 CLOCK. Hence, it seems possible that a key function of the LIN-42–KIN-20 complex in
415 the context of molting could be regulation of KIN-20 rather than LIN-42. Such a scenario

may also explain the previous observation that forced expression of the short LIN-42a isoform, largely comprising the CK1BD + Tail, caused extended molt durations (Monsalve *et al*, 2011), as this might sequester KIN-20 and/or inhibit its kinase activity.

Distinct functions of LIN-42 and KIN-20 in molting versus heterochronic timing?

Our data not only support the existence of LIN-42 and KIN-20 in a stable complex that is important for molting timing, but also indicate that LIN-42 and KIN-20 can function independently of one another in some contexts. Thus, we observed co-localization of the two proteins in the epidermis, but not in other tissues. Moreover, neither *kin-20(lf)* nor *lin-42(ΔCK1DB)* mutations cause precocious alae, a phenotype observed with several other *lin-42* mutant alleles. These findings agree with previous genetic data that suggested independent functions of *lin-42* and *kin-20* in regulating the expression of the heterochronic *let-7* microRNA (Rhodehouse *et al*, 2018). A recent study on LIN-42's function in regulating another heterochronic miRNA, *lin-4*, indicated that physical interaction with the NHR-85 transcription factor may support LIN-42's activity in this process, and perhaps the heterochronic pathway more generally (Kinney *et al*, 2023). Relatively mild effects upon *nhr-85* deletion, and LIN-42's ability to interact with additional transcription factors in a yeast two-hybrid assay suggest that additional functionally relevant interactions partners remain to be identified. The apparent differences in wiring among components of the heterochronic pathway and the molting timer may reflect their different modes of timekeeping where the heterochronic pathway is chiefly concerned with the order of events and the molting timer - similar to the circadian clock - with the tempo and/or robustness of their execution.

Finally, we note that the LIN-42 C-terminal tail, although heavily phosphorylated by CK1 *in vitro*, is dispensable for rhythmic molting but required for normal timing of alae formation. Whether this reflects a role of LIN-42–KIN-20 interaction in the heterochronic pathway that is anchoring independent, or a function of the tail that is independent of its phosphorylation, remains to be determined.

Conclusion

445 The components and wiring of the clock that controls rhythmic molting is only beginning
446 to be elucidated, and it appears that some of the main components may differ from that
447 of the circadian clock (Meeuse *et al*, 2023). Moreover, examination of factors that are
448 conserved between the heterochronic timer and the circadian clock e.g., LIN-42/PER,
449 NHR-23/RORa, and NHR-85/REV-ERB, suggested a different wiring among them
450 (Kinney *et al*, 2023; Rhodehouse *et al*, 2018). The LIN-42-KIN-20 complex uncovered
451 here is thus the first conserved module identified between the circadian clock and the
452 nematode molting timer. A potentially simplified function of LIN-42-KIN-20 may facilitate
453 future dissection of the mechanism of CK1 regulation by PER.
454

455 **Materials and Methods**

456 ***C. elegans* culture and genome editing**

457 *C. elegans* were grown and maintained at 20℃ and cultured as described (Brenner,
458 1974), except worms were grown on MYOB agar instead of NGM as described (Church
459 *et al*, 1995). Full genotypes of strains used in this work are listed in Table S2. All mutant
460 strains were backcrossed to N2 at least 2X. The Bristol N2 strain was used as wild
461 type. *lin-42* mutant strains used in this work were generated by injection of Cas9 or Cas12
462 ribonucleoprotein complexes as described (Ragle *et al*, 2022). Specified deletions were
463 made in the endogenous *lin-42* locus in N2 animals. Repair templates were used at 100
464 ng/µl along with Cas9 or Cas12 at 250 ng/µl, crRNA oligos at 60 ng/µl, and 10 ng/µl co-
465 injection marker (pCFJ90)(Frøkjaer-Jensen *et al*, 2008). Strains used in luciferase assays
466 were generated by crossing mutant strains with a previously described luciferase reporter
467 strain (HW1993) (Meeuse *et al*, 2020) (Table S2). *Lin-42* and *kin-20* tagged strains were
468 obtained using CRISPR as described previously (Ghanta & Mello, 2020)(cite). For *lin-42*,
469 a GFP::3xFLAG or 3xFLAG tag was inserted at the N-terminus of LIN-42b+c isoforms.
470 The *kin-20* tagged strains were obtained by inserting 3x::FLAG-HA or wrmScarlet at the
471 first common shared exon of all KIN-20 isoforms. In Table S3, we list oligo repair
472 templates and genotyping primers. In Table S4 we list crRNAs used.

473 **Immunoprecipitation**

474 For the 3xFLAG-LIN-42 IP, mixed stage animals were obtained by plating eggs after a
475 standard hypochlorite treatment and growth at different temperatures (15°C, 20°C and
476 25°C). After 24 hrs of plating, worms were collected by pooling 30,000 worms from each
477 temperature condition per strain and replicate (triplicates for each strain). For the HA-KIN-
478 20 IP, synchronized worms were collected after 32 hrs at 25°C. For the mapping of LIN-
479 42 phosphorylation sites, synchronized worms were grown at 25°C and collected hourly
480 from 14 hrs (L2 larval stage to 25 hrs (L4 larval stage). Worm extracts followed by
481 immunoprecipitation were done as previously described (Gudipati *et al*, 2021). In brief,
482 extracts were made in lysis buffer (50mM Tris-HCl, pH 7.5, 150 mM NaCl, 1% TRITON
483 X-100, 1 mM EDTA) supplemented with 1 mM PMSF and 1 tablet of cOmplete Protease
484 inhibitor (Roche, cat. No. 11 873 580 001) per 50 ml using a MP Biomedical Fast-Prep-
485 24 5G bead beater. For the FLAG IP, cleared worm extract was incubated with 50 µl of
486 50% bead suspension of anti-FLAG M2 Magnetic Beads (Sigma. Catalog Number
487 M8823) for 2 hours at 4°C. For the HA-IP worm extract was incubated with 50 µl of bead
488 suspension of Pierce™ Anti-HA Magnetic Beads (Thermo Scientific, Cat. No. 88837).

489 **Proteolytic digest**

490 The beads were incubated for 4 hrs at RT with 800 rpm shaking in 5 µl of digestion buffer
491 (3 M guanidine hydrochloride, 20 mM EPPS (4-(2-Hydroxyethyl)-1-
492 piperazinepropanesulfonic acid) pH 8.5, 10 mM CAA (2-Chloroacetamide), 5 mM TCEP
493 (Tris(2-carboxyethyl)phosphine hydrochloride)) and 1 µl of Lys-C (0.2 µg/µl in 50 mM
494 HEPES, pH 8.5). 1 µl of trypsin (0.2 µg/µl) was added and incubated at 37°C overnight.
495 After 12 hrs another 1 µl of trypsin was added and incubated for 4 more hours at 37°C

496 **Mass spectrometry to identify LIN-42 interacting factors**

497 The generated peptides were acidified with 0.8% TFA (final concentration) and analyzed
498 by LC–MS/MS on an EASY-nLC 1000 [Thermo Scientific] with a two-column set-up. The
499 peptides were applied onto a peptide 75µm x 2cm PepMap Trap trapping column [Thermo
500 Scientific] in 0.1% formic acid, 2% acetonitrile in H2O at a constant pressure of 800 bar.
501 Using a flow rate of 150 nl/min, peptides were separated on a 50 µm x 15 cm PepMap
502 C18, 2 µm, 100 A [Thermo Scientific] at 45 ˚C with a linear gradient of 2%–6% buffer B

503 in buffer A in 3 min followed by a linear increase from 6 to 22% in 40 min, 22%–28% in 9
504 min, 28%–36% in 8 min, 36%–80% in 1 min, and the column was finally washed for 14
505 min at 80% buffer B in buffer A (buffer A: 0.1% formic acid; buffer B: 0.1% formic acid in
506 acetonitrile). The separation column was mounted on an EASY-Spray™ source [Thermo
507 Scientific] connected to an Orbitrap Fusion LUMOS [Thermo Scientific]. The data were
508 acquired using 120,000 resolution for the peptide measurements in the Orbitrap and a
509 top T (3 s) method with HCD fragmentation for each precursor and fragment
510 measurement in the ion trap according the recommendation of the manufacturer (Thermo
511 Scientific). For the analysis protein identification and relative quantification of the proteins
512 was performed with MaxQuant v.1.5.3.8 using Andromeda as search engine, and label-
513 free quantification (LFQ). The *C. elegans* subset of the UniProt v.2021_05 combined with
514 the contaminant database from MaxQuant was searched and the protein and peptide
515 FDR were set to 0.01. The LFQ intensities estimated by MaxQuant were analyzed with
516 the einprot R package (https://github.com/fmicompbio/einprot) v0.5.4. Features classified
517 by MaxQuant as potential contaminants or reverse (decoy) hits or identified only by site,
518 as well as features identified based on a single peptide or with a score below 10, were
519 filtered out. The LFQ intensities were log2 transformed and missing values were imputed
520 using the 'MinProb' method from the imputeLCMD R package v2.0 with default settings.
521 Pairwise comparisons were performed using limma v3.50.0, considering only features
522 with at least 2 non-imputed values across all the samples in the comparison. Estimated
523 log2-fold changes and P-values (moderated t-test) from limma were used to construct
524 volcano plots.

525 **Mass spectrometry to map *in vivo* LIN-42 phosphorylation sites**

526 The peptides from each sample were labeled with TMTpro reagents and pooled. The TMT
527 labeled peptide mixture was subjected to off-line high pH fractionation on a YMC Triart
528 C18 0.5 × 250 mm column (YMC Europe GmbH) using the Agilent 1100 system (Agilent
529 Technologies). A total of 96 fractions was collected for each experiment and
530 concatenated into 48 fractions as previously described. For each LC-MS analysis, all
531 available peptides were loaded onto a PepMap Neo trap (Thermo Fisher) using the
532 Vanquish Neo UHPLC system (Thermo Fisher). On-line peptide separation was

533 performed on a 15-cm EASY-Spray™ C18 column (ES75150PN, Thermo Fisher) by
534 applying a linear gradient of increasing ACN concentration at a flowrate of 200 nL/min.
535 Orbitrap Fusion Lumos Tribrid (Thermo Fisher) mass spectrometer was operated in the
536 data-dependent mode. The ions for the survey scan were collected for a maximum of 50
537 ms to reach the standard AGC target value and the scan recorded using an Orbitrap
538 detector at a resolution of 120'000. The topmost intense precursor ions from the Orbitrap
539 survey scan recorded every 3 sec were selected for stepped higher-energy C-trap
540 dissociation (HCD) at 29%, 32% and 35% normalized collision energy scan. To reach an
541 AGC value of 100'000 ions, the maximum ion accumulation time for the MS2 scan was
542 set to 500ms. The TMT reporter ions were quantified using an MS2 scan recorded using
543 the Orbitrap analyzer at a resolution of 50'000. Thermo RAW files were processed using
544 Proteome Discoverer 2.4 software (Thermo Fisher) as described in the manufacturer's
545 instructions. Briefly, the Sequest search engine was used to search the MS2 spectra
546 against the C. elegans UniProt database (downloaded on 05/2023) supplemented with
547 common contaminating proteins. For peptide identification, cysteine
548 carbamidomethylation and TMTpro tags on lysine and peptide N-termini were set as static
549 modifications, whereas oxidation of methionine residues and acetylation protein N-termini
550 were set as variable modifications. The assignments of the MS2 scans were filtered to
551 allow 1% FDR. For reporter quantification, the S/N values were corrected for isotopic
552 impurities of the TMTpro reagent using the values provided by the manufacturer. The
553 sums across all TMTpro reporter channels were normalized assuming equal total protein
554 content in each sample.

555 **Western Blot**

556 Synchronized animals were collected hourly from 13 hrs - 23 hrs after plating at 25°C.
557 Extracts were made by boiling at 95°C for 5 minutes in lysis buffer (63 mM Tris-HCl (pH
558 6.8), 5 mM DTT, 2% SDS, 5% sucrose) followed by sonication with a BioRupter Plus
559 (Diagnode) with the following settings: 13 cycles, 30 s on/off at 4°C. Samples were
560 cleared by centrifugation, before separating proteins by SDS-PAGE (loading: 50 µg
561 protein extract per well) and transferring them to PVDF membranes by semi-dry blotting.
562 The following antibodies were used: Monoclonal mouse anti-FLAG M2-Peroxidase (HRP)

563 (Sigma-Aldrich; A8592, dilution: 1:1000), monoclonal mouse anti-Actin clone C4
564 (Millipore; MAB1501, dilution 1:7500) and anti-mouse HRP conjugated antibody (GE
565 Healthcare #NXA931, dilution 1:2000). The membrane was incubated with ECL™ Prime
566 Western-Blot-Reagent (Cytiva,#RPN2236) and bands detected with an Amersham
567 Imager 680 (GE Healthcare).

568 **Phenotypic analysis**

569 For phenotypic analyses, gravid adults were bleached, and embryos were hatched at low
570 density onto plates seeded with OP50, or gravid adults were picked onto seeded plates
571 and removed after 1-2 hours. Animals were maintained at 20°C and observed daily or
572 twice daily. Bag-of-worms phenotype was determined when live progeny were observed
573 inside adult animals. For brood counts, animals were individually transferred to fresh wells
574 daily for five days after L4 and live progeny were counted and averaged. Statistical
575 significance was determined using a two-tailed unpaired Student's t-test. $P < 0.05$ was
576 considered statistically significant. **** indicates $P < 0.0001$.

577 **Imaging**

578 To score premature alae, synchronized animals were collected from MYOB plates by
579 washing off plates. 1000 µl of M9 + 2% gelatin was added to the plate or well, agitated to
580 suspend animals in M9+gelatin, and then transferred to a 1.5 ml tube. Animals were spun
581 at 700xg for 1 min. The media was then aspirated off and animals were resuspended in
582 500µl M9 + 2% gelatin with 5 mM levamisole. 12 µl of animals in M9 +gel with levamisole
583 solution were placed on slides with a 2% agarose pad and secured with a coverslip.
584 Images were acquired using a Plan-Apochromat 40x/1.3 Oil DIC lens or a Plan-
585 Apochromat 63x/1.4 Oil DIC lens on an AxioImager M2 microscope (Carl Zeiss
586 Microscopy, LLC) equipped with a Colibri 7 LED light source and an Axiocam 506 mono
587 camera. Acquired images were processed through Affinity photo software (version:
588 1.9.2.1035). For the confocal microscopy, L3/L4 stage-animals were picked from OP50
589 plates grown at 25°C. Worms were mounted on a glass slide with a 2 % agarose patch
590 immobilized with 5 µl levamisole 10 mM (Fluca Analytical, #31742). Images were acquired
591 in channels for red (561 nm laser), green (488 nm laser) and DIC with a 40x/1.3 immersion

592 objective on a Zeiss LSM700 confocal microscope. Acquired images were processed with
593 FiJi (Schindelin *et al*, 2012).

594

595 **Luciferase assays**

596 Assays were performed and analyzed as described (Meeuse *et al*, 2020). Briefly, gravid
597 adults were bleached, and eggs were immediately singled into wells containing 90 µl
598 OP50/S-Basal/D-Luciferin solution per well and left in the luminometer machine and
599 measured every 10 minutes for 0.5 seconds. The assays lasted 96 hrs or 130 hrs. For
600 statistical analysis, we performed a Wilcoxon-Mann-Whitney test (implemented in the
601 python package SciPy version 1.4.1 as the function Mann-Whitney-U).

602

603 **Expression and purification of recombinant proteins**

604 All proteins were expressed from a pET22-based vector in *Escherichia coli* Rosetta (DE3)
605 cells based on the Parallel vector series (Sheffield *et al*, 1999). All LIN-42 constructs
606 (CK1BD + Tail, residues 402-598; CK1BD, residues 402-475; CK1BD-ΔA, -ΔB, and ΔAB
607 mutants) were expressed downstream of an N-terminal TEV-cleavable His-NusA tag.
608 Human CK1δ catalytic domains (CK1δ ΔC, residues 1–317) were all expressed with a
609 TEV-cleavable His-GST tag. All proteins expressed from Parallel vectors have an
610 additional N-terminal vector artifact of 'GAMDPEF' remaining after TEV cleavage. Cells
611 were grown in LB media at 37°C until the O.D.600 reached ~0.8; expression was induced
612 with 0.5 mM IPTG, and cultures were grown for approximately 16–20 hours more at 18°C.
613 Cells were centrifuged at 3,200 x g, resuspended in 50 mM Tris, pH 7.5, 300 mM NaCl,
614 20 mM imidazole, 5% (vol/vol) glycerol, 1 mM tris(2-carboxyethyl)phosphine (TCEP), and
615 0.05% Tween-20. For purification of recombinant protein, cells were lysed with a
616 microfluidizer followed by sonication and then the lysate was clarified via centrifugation
617 at 140,500 x g for 1 hour at 4ºC. Ni-NTA affinity chromatography was used to extract his-
618 tagged proteins from the lysate and then the affinity/solubility tags were cleaved using
619 His6-TEV (GST-TEV for CK1δ ΔC) protease overnight at 4ºC. The cleaved protein was

620 then separated from solubility tag and TEV by a second Ni-NTA (GST for CK1δ ΔC)
621 affinity column and further purified using size exclusion chromatography (SEC) in 50 mM
622 Tris, pH 7.5, 200 mM NaCl, 1 mM EDTA, 5% (vol/vol) glycerol, 1 mM TCEP, and 0.05%
623 Tween-20. Small aliquots of protein were frozen in liquid nitrogen and stored at -70ºC for
624 long-term storage.

625 ***In vitro* biotinylation, pull-down assays, and bio-layer interferometry**

626 LIN-42 CK1BD + Tail constructs and CK1δ ΔC were biotinylated via Sortase A-mediated
627 reactions between a Sortase A recognition motif peptide (biotin-LPETGG) and our LIN-
628 42 CK1BD + Tail/CK1δ ΔC (N-terminal G from 'GAMDPEF' artifact). Reactions were
629 carried out in 50 mM Tris pH 7.5 and 150 mM NaCl using 5 μM His6-Sortase A, 300 μM
630 biotin-LPETGG, and 50 μM protein. Ni-NTA affinity chromatography followed by SEC was
631 used to purify labeled protein from His6-Sortase A and excess biotin, respectively. Pull
632 down assays were performed using magnetic streptavidin beads to bind biotinylated LIN-
633 42 CK1BD + Tail WT and mutants (final concentration 5 μM) in the presence and absence
634 of CK1δ ΔC (final concentration 5 μM). All BLI assays were performed in SEC buffer
635 supplemented with 7.5mM BSA as previously described (Fribourgh *et al*, 2020; Parico *et*
636 *al*, 2020) using an eight-channel Octet-RED96e.

637 **ADP-Glo kinase assays**

638 Substrate titration kinase reactions were performed on the indicated recombinant LIN-42
639 proteins (CK1BD + Tail WT or mutants) using the ADP-Glo kinase assay kit (Promega)
640 according to the manufacturer's instructions. All reactions were performed in 30 μL
641 volumes in duplicate (n=3 independent experiments) using 1x kinase buffer (25mM Tris
642 pH 7.5, 100mM NaCl, 10mM $MgCl_2$, and 2mM TCEP) supplemented with 100 μM ATP,
643 0.2 μM recombinant CK1, and indicated LIN-42 proteins. Reactions were held at room
644 temperature for 1-hour and then 5 μL aliquots were taken and quenched with ADP-Glo
645 reagents. Luminescent measurements were measured at room temperature with a
646 SYNERGY2 microplate reader in 384-well microplates. Data analysis was performed
647 using Excel (Microsoft) and Prism (GraphPad).

648 **^{32}P-ATP kinase assays**

649 1 μM human CK1δ ΔC was incubated with 10 μM LIN-42 (CK1BD + Tail/CK1BD WT and
650 mutant proteins) in 1x kinase buffer (25 mM Tris pH 7.5, 100 mM NaCl, 10 mM MgCl2, 2
651 mM TCEP). Reactions were started by the addition of ^{32}P-ATP (final concentration 2 mM)
652 and samples were collected at indicated time points and quenched in an equivalent
653 volume of 2x SDS-PAGE loading buffer. Proteins labeled with ^{32}P were separated and
654 analyzed via SDS-PAGE and the gels were dried at 80ºC for 2-hours before overnight
655 exposure in a phosphor screen (Amersham Biosciences). A Typhoon Trio (Amersham
656 Biosciences) phosphorimager was used to visualize exposed gels and ^{32}P-labeled protein
657 bands were quantified via densitometry using ImageJ (NIH), Excel (Microsoft) and Prism
658 (GraphPad).

659 ***In vitro* Mass Spectrometry**

660 Kinase reactions were performed in 1x kinase buffer (25 mM Tris pH 7.5, 100 mM NaCl,
661 10 mM MgCl2, 2 mM TCEP) for 60 minutes and then quenched with 20 mM EDTA.
662 Samples were denatured, reduced, alkylated, and digested according to the In-solution
663 Protein Digestion (Promega) protocol. In brief, phosphorylated samples were
664 denatured/reduced in 8M urea/50mM ammonium bicarbonate/5mM Dithiothreitol (DTT)
665 for 1hr at 37°C. Samples were incubated for 30 minutes in the dark with 15mM
666 iodoacetamide and then digested with MS-Grade Modified Trypsin according to the
667 Trypsin Digestion Protocol (Promega). Digested Samples were phospho-enriched using
668 the High-Select Fe-NTA Phosphopeptide Enrichment Kit (Thermo Scientific) and sent for
669 analysis at the University of California, Davis Proteomic Core Facility.

670

671 **Author contributions**

672 **Rebecca K. Spangler:** Conceptualization; formal analysis; investigation; writing –
673 original draft. **Guinevere E. Ashley:** Conceptualization; formal analysis; investigation;
674 writing – original draft. **Kathrin Braun:** Conceptualization; Formal analysis; investigation;
675 writing – review and editing. **Daniel Wruck:** Formal analysis; investigation; writing –

review and editing. **Andrea Ramos-Coronado:** Formal analysis; investigation; writing – review and editing. **James Matthew Ragle:** Formal analysis; investigation; writing – review and editing. **Vytautas Iesmantavicius:** Formal analysis; investigation; writing – review and editing. **Daniel Hess:** Formal analysis; investigation; writing – review and editing. **Carrie L. Partch:** Conceptualization; supervision; funding acquisition; writing – review and editing; project administration. **Helge Großhans:** Conceptualization; supervision; funding acquisition; writing – original draft; project administration. **Jordan D. Ward:** Conceptualization; supervision; funding acquisition; writing – original draft; project administration.

Acknowledgements

Some strains were provided by the *Caenorhabditis* Genetics Center, which is funded by the NIH Office of Research Infrastructure Programs [P40 OD010440]. We thank Iskra Katic for worm injections and technical support and Dimos Gaidatzis for help with proteomics data analysis. We are thankful to Laurent Gelman and Laure Plantard for help with confocal imaging. Analysis for this project was performed in the UC Davis Campus Mass Spectrometry Facilities, with instrument funding provided by the NIH (S10OD026918-01A1).

Funding

This work was funded by the National Institutes of Health (NIH) National Institute of General Medical Sciences (NIGMS) to J.D.W (R01GM138701) and C.L.P. (R35GM141849). This work is part of a project that has received funding from the European Research Council (ERC) under the European Union's Horizon 2020 research and innovation program (Grant agreement No. 741269, to H.G.) and from the Swiss National Science Foundation (#310030_207470, to H.G.). The FMI is core-funded by the Novartis Research Foundation.

704 **Data availability**

705 All relevant data can be found within the article and its supplementary information.

706

707 **References**

708 Abrahante JE, Miller EA & Rougvie AE (1998) Identification of Heterochronic Mutants in
709 *Caenorhabditis elegans*: Temporal Misexpression of a Collagen::Green
710 Fluorescent Protein Fusion Gene. *Genetics* 149: 1335–1351
711 Akashi M, Tsuchiya Y, Yoshino T & Nishida E (2002) Control of Intracellular Dynamics
712 of Mammalian Period Proteins by Casein Kinase I ε (CKIε) and CKIδ in Cultured
713 Cells. *Mol Cell Biol* 22: 1693–1703
714 Ambros V (1989) A hierarchy of regulatory genes controls a larva-to-adult
715 developmental switch in *C. elegans*. *Cell* 57: 49–57
716 Ambros V & Horvitz HR (1984) Heterochronic mutants of the nematode *Caenorhabditis*
717 *elegans*. *Science* 226: 409–416
718 An Y, Yuan B, Xie P, Gu Y, Liu Z, Wang T, Li Z, Xu Y & Liu Y (2022) Decoupling PER
719 phosphorylation, stability and rhythmic expression from circadian clock function
720 by abolishing PER-CK1 interaction. *Nat Commun* 13: 3991
721 Aryal RP, Kwak PB, Tamayo AG, Gebert M, Chiu P-L, Walz T & Weitz CJ (2017)
722 Macromolecular Assemblies of the Mammalian Circadian Clock. *Mol Cell* 67:
723 770-782.e6
724 Banerjee D, Kwok A, Lin S-Y & Slack FJ (2005) Developmental timing in *C. elegans* is
725 regulated by *kin-20* and *tim-1*, homologs of core circadian clock genes. *Dev Cell*
726 8: 287–295
727 Brenner S (1974) The genetics of *Caenorhabditis elegans*. *Genetics* 77: 71–94
728 Cao X, Yang Y, Selby CP, Liu Z & Sancar A (2021) Molecular mechanism of the
729 repressive phase of the mammalian circadian clock. *Proc Natl Acad Sci U S A*
730 118: e2021174118
731 Chiou Y-Y, Yang Y, Rashid N, Ye R, Selby CP & Sancar A (2016) Mammalian Period
732 represses and de-represses transcription by displacing CLOCK-BMAL1 from
733 promoters in a Cryptochrome-dependent manner. *Proc Natl Acad Sci U S A* 113:
734 E6072–E6079
735 Church DL, Guan KL & Lambie EJ (1995) Three genes of the MAP kinase cascade,
736 *mek-2*, *mpk-1/sur-1* and *let-60 ras*, are required for meiotic cell cycle progression
737 in *Caenorhabditis elegans*. *Development* 121: 2525–2535
738 Crosby P, Goularte NF, Sharma D, Chen E, Parico GCG, Philpott JM, Harold R,
739 Gustafson CL & Partch CL (2023) CHRONO participates in multi-modal
740 repression of circadian transcriptional complexes. 2022.10.04.510902
741 doi:10.1101/2022.10.04.510902 [PREPRINT]
742 Cullati SN, Chaikuad A, Chen J-S, Gebel J, Tesmer L, Zhubi R, Navarrete-Perea J,
743 Guillen RX, Gygi SP, Hummer G, *et al* (2022) Kinase domain
744 autophosphorylation rewires the activity and substrate specificity of CK1
745 enzymes. *Mol Cell* 82: 2006-2020.e8

Dahlberg CL, Nguyen EZ, Goodlett D & Kimelman D (2009) Interactions between Casein Kinase Iε (CKIε) and Two Substrates from Disparate Signaling Pathways Reveal Mechanisms for Substrate-Kinase Specificity. *PLOS ONE* 4: e4766

Edelman TLB, McCulloch KA, Barr A, Frøkjær-Jensen C, Jorgensen EM & Rougvie AE (2016) Analysis of a *lin-42/period* Null Allele Implicates All Three Isoforms in Regulation of *Caenorhabditis elegans* Molting and Developmental Timing. *G3 GenesGenomesGenetics* 6: 4077–4086

Eide EJ, Woolf MF, Kang H, Woolf P, Hurst W, Camacho F, Vielhaber EL, Giovanni A & Virshup DM (2005) Control of mammalian circadian rhythm by CKIepsilon-regulated proteasome-mediated PER2 degradation. *Mol Cell Biol* 25: 2795–2807

Fribourgh JL, Srivastava A, Sandate CR, Michael AK, Hsu PL, Rakers C, Nguyen LT, Torgrimson MR, Parico GCG, Tripathi S, *et al* (2020) Dynamics at the serine loop underlie differential affinity of cryptochromes for CLOCK:BMAL1 to control circadian timing. *eLife* 9: e55275

Frøkjaer-Jensen C, Davis MW, Hopkins CE, Newman BJ, Thummel JM, Olesen S-P, Grunnet M & Jorgensen EM (2008) Single-copy insertion of transgenes in *Caenorhabditis elegans*. *Nat Genet* 40: 1375–1383

Gallego M & Virshup DM (2007) Post-translational modifications regulate the ticking of the circadian clock. *Nat Rev Mol Cell Biol* 8: 139–148

Gebel J, Tuppi M, Chaikuad A, Hötte K, Schröder M, Schulz L, Löhr F, Gutfreund N, Finke F, Henrich E, *et al* (2020) p63 uses a switch-like mechanism to set the threshold for induction of apoptosis. *Nat Chem Biol* 16: 1078–1086

Gekakis N, Staknis D, Nguyen HB, Davis FC, Wilsbacher LD, King DP, Takahashi JS & Weitz CJ (1998) Role of the CLOCK protein in the mammalian circadian mechanism. *Science* 280: 1564–1569

Ghanta KS & Mello CC (2020) Melting dsDNA Donor Molecules Greatly Improves Precision Genome Editing in *Caenorhabditis elegans*. *Genetics* 216: 643–650

Gissendanner CR, Crossgrove K, Kraus KA, Maina CV & Sluder AE (2004) Expression and function of conserved nuclear receptor genes in *Caenorhabditis elegans*. *Dev Biol* 266: 399–416

Gudipati RK, Braun K, Gypas F, Hess D, Schreier J, Carl SH, Ketting RF & Großhans H (2021) Protease-mediated processing of Argonaute proteins controls small RNA association. *Mol Cell* 81: 2388-2402.e8

Harold R, Tulsian NK, Narasimamurthy R, Yaitanes N, Hernandez MGA, Lee H-W, Virshup DM & Partch CL (2023) Isoform-specific C-terminal phosphorylation drives autoinhibition of Casein Kinase 1. 2023.04.24.538174 doi:10.1101/2023.04.24.538174 [PREPRINT]

Hasegawa K, Saigusa T & Tamai Y (2005) *Caenorhabditis elegans* opens up new insights into circadian clock mechanisms. *Chronobiol Int* 22: 1–19

Hendriks G-J, Gaidatzis D, Aeschimann F & Großhans H (2014) Extensive oscillatory gene expression during *C. elegans* larval development. *Mol Cell* 53: 380–392

Jeon M, Gardner HF, Miller EA, Deshler J & Rougvie AE (1999) Similarity of the *C. elegans* Developmental Timing Protein LIN-42 to Circadian Rhythm Proteins. *Science* 286: 1141–1146

Jones CR, Campbell SS, Zone SE, Cooper F, DeSano A, Murphy PJ, Jones B, Czajkowski L & Ptček LJ (1999) Familial advanced sleep-phase syndrome: A short-period circadian rhythm variant in humans. *Nat Med* 5: 1062–1065

Kim EY, Ko HW, Yu W, Hardin PE & Edery I (2007) A DOUBLETIME kinase binding domain on the *Drosophila* PERIOD protein is essential for its hyperphosphorylation, transcriptional repression, and circadian clock function. *Mol Cell Biol* 27: 5014–5028

Kinney B, Sahu S, Stec N, Hills-Muckey K, Adams DW, Wang J, Jaremko M, Joshua-Tor L, Keil W & Hammell CM (2023) A circadian-like gene network programs the timing and dosage of heterochronic miRNA transcription during *C. elegans* development. *Dev Cell* 58: 2563-2579.e8

Kostrouchova M, Krause M, Kostrouch Z & Rall JE (1998) CHR3: a *Caenorhabditis elegans* orphan nuclear hormone receptor required for proper epidermal development and molting. *Development* 125: 1617–1626

Lamberti ML, Spangler RK, Cerdeira V, Ares M, Rivollet L, Ashley GE, Coronado AR, Tripathi S, Spiousas I, Ward JD, *et al* (2023) Regulation of the circadian clock in *C. elegans* by clock gene homologs *kin-20* and *lin-42*. 2023.04.13.536481 doi:10.1101/2023.04.13.536481 [PREPRINT]

Lažetić V & Fay DS (2017) Molting in *C. elegans*. *Worm* 6: 1–20

Lee C, Etchegaray JP, Cagampang FR, Loudon AS & Reppert SM (2001) Posttranslational mechanisms regulate the mammalian circadian clock. *Cell* 107: 855–867

Liu Z (1990) Genetic Control of Stage-specific Developmental Events in *C. elegans*.

Lowrey PL, Shimomura K, Antoch MP, Yamazaki S, Zemenides PD, Ralph MR, Menaker M & Takahashi JS (2000) Positional syntenic cloning and functional characterization of the mammalian circadian mutation tau. *Science* 288: 483–492

Lowrey PL & Takahashi JS (2011) Genetics of circadian rhythms in Mammalian model organisms. *Adv Genet* 74: 175–230

Marzoll D, Serrano FE, Shostak A, Schunke C, Diernfellner ACR & Brunner M (2022) Casein kinase 1 and disordered clock proteins form functionally equivalent, phospho-based circadian modules in fungi and mammals. *Proc Natl Acad Sci U A* 119

McCulloch KA & Rougvie AE (2014) *Caenorhabditis elegans period* homolog *lin-42* regulates the timing of heterochronic miRNA expression. *Proc Natl Acad Sci* 111: 15450–15455

Meeuse MW, Hauser YP, Morales Moya LJ, Hendriks G, Eglinger J, Bogaarts G, Tsiairis C & Großhans H (2020) Developmental function and state transitions of a gene expression oscillator in *Caenorhabditis elegans*. *Mol Syst Biol* 16: e9975

Meeuse MWM, Hauser YP, Nahar S, Smith AAT, Braun K, Azzi C, Rempfler M & Großhans H (2023) *C. elegans* molting requires rhythmic accumulation of the Grainyhead/LSF transcription factor GRH-1. *EMBO J* n/a: e111895

Migliori ML, Goya ME, Lamberti ML, Silva F, Rota R, Bénard C & Golombek DA (2023) *Caenorhabditis elegans* as a Promising Model Organism in Chronobiology. *J Biol Rhythms*: 07487304221143483

Monsalve GC, Van Buskirk C & Frand AR (2011) LIN-42/PERIOD controls cyclical and developmental progression of *C. elegans* molts. *Curr Biol CB* 21: 2033–2045

Narasimamurthy R, Hunt SR, Lu Y, Fustin J-M, Okamura H, Partch CL, Forger DB, Kim JK & Virshup DM (2018) CK1δ/ε protein kinase primes the PER2 circadian phosphoswitch. *Proc Natl Acad Sci U S A* 115: 5986–5991

Nawathean P, Stoleru D & Rosbash M (2007) A small conserved domain of *Drosophila* PERIOD is important for circadian phosphorylation, nuclear localization, and transcriptional repressor activity. *Mol Cell Biol* 27: 5002–5013

Olmedo M, O'Neill JS, Edgar RS, Valekunja UK, Reddy AB & Merrow M (2012) Circadian regulation of olfaction and an evolutionarily conserved, nontranscriptional marker in *Caenorhabditis elegans*. *Proc Natl Acad Sci*

Parico GCG, Perez I, Fribourgh JL, Hernandez BN, Lee H-W & Partch CL (2020) The human CRY1 tail controls circadian timing by regulating its association with CLOCK:BMAL1. *Proc Natl Acad Sci U S A* 117: 27971–27979

Perales R, King DM, Aguirre-Chen C & Hammell CM (2014) LIN-42, the *Caenorhabditis elegans* PERIOD homolog, Negatively Regulates MicroRNA Transcription. *PLoS Genet* 10: e1004486

Philpott JM, Freeberg AM, Park J, Lee K, Ricci CG, Hunt SR, Narasimamurthy R, Segal DH, Robles R, Cai Y, *et al* (2023) PERIOD phosphorylation leads to feedback inhibition of CK1 activity to control circadian period. *Mol Cell* 83: 1677-1692.e8

Philpott JM, Narasimamurthy R, Ricci CG, Freeberg AM, Hunt SR, Yee LE, Pelofsky RS, Tripathi S, Virshup DM & Partch CL (2020) Casein kinase 1 dynamics underlie substrate selectivity and the PER2 circadian phosphoswitch. *eLife* 9: e52343

Preußner M & Heyd F (2016) Post-transcriptional control of the mammalian circadian clock: implications for health and disease. *Pflugers Arch* 468: 983–991

Ragle JM, Levenson MT, Clancy JC, Vo AA, Pham V & Ward JD (2022) The conserved, secreted protease inhibitor MLT-11 is necessary for *C. elegans* molting and embryogenesis. 2022.06.29.498124 doi:10.1101/2022.06.29.498124 [PREPRINT]

Rhodehouse K, Cascino K, Aseltine L, Padula A, Weinstein R, Spina JS, Olivero CE & Van Wynsberghe PM (2018) The Doubletime Homolog KIN-20 Mainly Regulates *let-7* Independently of Its Effects on the Period Homolog LIN-42 in *Caenorhabditis elegans*. *G3 Bethesda Md* 8: 2617–2629

Rüegger S, Miki TS, Hess D & Großhans H (2015) The ribonucleotidyl transferase USIP-1 acts with SART3 to promote U6 snRNA recycling. *Nucleic Acids Res* 43: 3344–3357

Schindelin J, Arganda-Carreras I, Frise E, Kaynig V, Longair M, Pietzsch T, Preibisch S, Rueden C, Saalfeld S, Schmid B, *et al* (2012) Fiji: an open-source platform for biological-image analysis. *Nat Methods* 9: 676–682

Sheffield P, Garrard S & Derewenda Z (1999) Overcoming expression and purification problems of RhoGDI using a family of 'parallel' expression vectors. *Protein Expr Purif* 15: 34–39

Shirogane T, Jin J, Ang XL & Harper JW (2005) SCFbeta-TRCP controls clock-dependent transcription via casein kinase 1-dependent degradation of the mammalian period-1 (Per1) protein. *J Biol Chem* 280: 26863–26872

Takahashi JS (2017) Transcriptional architecture of the mammalian circadian clock. *Nat Rev Genet* 18: 164–179

882 Tennessen JM, Gardner HF, Volk ML & Rougvie AE (2006) Novel heterochronic
883 functions of the *Caenorhabditis elegans* period-related protein LIN-42. *Dev Biol*
884 289: 30–43
885 Toh KL, Jones CR, He Y, Eide EJ, Hinz WA, Virshup DM, Ptácek LJ & Fu YH (2001) An
886 hPer2 phosphorylation site mutation in familial advanced sleep phase syndrome.
887 *Science* 291: 1040–1043
888 Xu Y, Padiath QS, Shapiro RE, Jones CR, Wu SC, Saigoh N, Saigoh K, Ptácek LJ & Fu
889 Y-H (2005) Functional consequences of a CKIdelta mutation causing familial
890 advanced sleep phase syndrome. *Nature* 434: 640–644
891 Xu Y, Toh KL, Jones CR, Shin J-Y, Fu Y-H & Ptácek LJ (2007) Modeling of a human
892 circadian mutation yields insights into clock regulation by PER2. *Cell* 128: 59–70
893 Zheng B, Larkin DW, Albrecht U, Sun ZS, Sage M, Eichele G, Lee CC & Bradley
894 A (1999) The *mPer2* gene encodes a functional component of the mammalian
895 circadian clock. *Nature* 400: 169–173
896